

Journal of Molecular Structure
Light-Triggered Click Reaction to Fabricate Bright Bovine Serum Albumin Encapsulates Photosensitizer's Nanoparticles for Effective Photodynamic Therapy of Melanoma Cells
--Manuscript Draft--

Manuscript Number:	MOLSTRUCT-D-25-04896R2
Article Type:	Research Paper
Section/Category:	Materials science
Keywords:	Aggregation-Induced Emission; Click reaction; Photodynamic Therapy; Bovine serum albumin; melanoma cell
Corresponding Author:	Muzhou Teng Lanzhou University CHINA
First Author:	Yifan Li
Order of Authors:	Yifan Li Yitao Fan Qian Liu Xuya Wang Yuxia Jin Muzhou Teng
Abstract:	Photodynamic therapy (PDT) has emerged as a promising anticancer strategy due to its non-invasive nature and precise spatiotemporal control. However, conventional photosensitizers (PSs) suffer from aggregation-caused quenching (ACQ), poor hydrophilicity, and serious oxygen dependence, limiting their clinical utility. To address these challenges, we developed a green and efficient strategy to fabricate hydrophilic aggregation-induced emission (AIE)-active Bovine Serum Albumin (BSA) Encapsulates PSs via an effective light-mediated thiol-yne click reaction. By designing alkynyl-functionalized AIE-active PSs with strong generating capability of type I/II reactive oxygen species (ROS), we achieved fast combination with thiol-rich BSA under UV light irradiation, forming stable BSA@AIE-active PSs' nanoparticles (NPs). The resulting NPs exhibited excellent water dispersibility, bright fluorescence and intense ROS generation. In vitro studies demonstrated their outstanding PDT effect to B16-F10 cancer cells under white light irradiation. This work proposed a universal, scalable, and eco-friendly platform for constructing AIE-active hydrophilic PS's NPs, overcoming longstanding hurdles in PS's hydrophobicity and fabrication complexity.

July 29, 2025

Dear Editor,

We wish to submit our *revised article* for your consideration by **JOURNAL OF MOLECULAR STRUCTURE**. We promise that this work is original and has not been published elsewhere, nor is it currently under consideration for publication elsewhere.

○ **Manuscript title**

Light-Triggered Click Reaction to Fabricate Bright Bovine Serum Albumin Encapsulates Photosensitizer's Nanoparticles for Effective Photodynamic Therapy of Melanoma Cells

○ **Manuscript authors**

Yifan Li, Yitao Fan, Qian Liu, Xuya Wang, Yuxia Jin, Muzhou Teng*

Address of corresponding author

Prof. Muzhou Teng, Department of Dermatology, The Second Hospital & Clinical Medical School, Lanzhou University; Gansu Provincial Maternity and Child-Care Hospital (Gansu Provincial Central Hospital), Lanzhou, China. E-mail: smutmz@126.com

○ **Justification**

Photodynamic therapy (PDT), as a non-invasive and spatiotemporally controllable treatment technology, has attracted increasing research interests in biomedical field. However, some disadvantages of conventional PSs make them difficult to achieve highly efficient practical applications, such as typical and head-scratching aggregation-caused quenching (ACQ) effect, poor water solubility, and serious oxygen dependence. These drawbacks often lead to reduced fluorescence and ROS generation efficiency, suboptimal biocompatibility, and limited therapeutic efficiency.

In recent years, aggregation-induced emission (AIE)-active PSs have emerged as a revolutionary class of PSs, addressing effectively the ACQ problem by exhibiting enhanced luminescence and ROS generation in the aggregated state. Despite their a series of advantages, the hydrophobic nature of most aromatic AIE-active PSs poses challenges in achieving stable aqueous dispersion, necessitating additional chemical modifications or carrier systems to improve biocompatibility.

Click chemistry, renowned for its high efficiency, selectivity, and mild reaction conditions, has become an important protocol to fabricate biomedical materials and modify surface, which has promising applications in the fields of bioconjugation and nanomaterial engineering. in this research work, two type Bovine Serum Albumin (BSA) encapsulated AIE-active PSs' NPs were designed and prepared based on a universal and eco-friendly light trigger thiol-yne click reaction method, which achieved great photodynamic therapy effect for the B16-F10 cancer cells. This work proposed a feasible and eco-friendly method for constructing hydrophilic AIE-active PS's NPs, which is expected to show huge promising potential for future biomedical applications.

We believe that this fundamental research is suitable to be published in the ***JOURNAL OF MOLECULAR STRUCTURE***, and will draw much attention from researchers working on the exploration of bright AIE-active PS's nanoparticles for future antitumor application.

Thank you for your consideration. We look forward to hearing from you.

Yours sincerely,

Prof. Muzhou Teng

Revision to MOLSTRUC-D-25-04896-R2 one by one

Dear Prof. Luca Evangelisti,

Thank you for your email. We have read the reviewers' comments and carefully revised our manuscript according to the reviewers' suggestions. The changes we made are highlighted in the text for your easy reference. Additionally, the revised manuscript with two forms (marked one and unmarked one) was uploaded.

The followings are our point-by-point responses to the reviewers' comments and suggestions.

Reviewer #2: The manuscript was adequately modified by the authors. I thought that it can be accepted in current form.

Reply: Thank you for recognition.

Reviewer #3: The authors have solved almost all the problems raised, and the scientific quality of this work has been improved. The following two minor points should be addressed before acceptable for publication in this journal:

Q1. In the synthesis part, the description of "DMSO" should be changed to "d6-DMSO" or "DMSO-d6".

Reply: Thank you for reminder. We correct this mistake in the revised file of supporting information with highlight words (Page 3-4).

Q2. The triple bands of alkynes in all chemical structures need to be linear.

Reply: Thank you for professional suggestion. We correct this mistake in the revised supporting information (Page 9-11, Figure S3-8).

Light-Triggered Click Reaction to Fabricate Bright Bovine Serum Albumin Encapsulates Photosensitizer's Nanoparticles for Effective Photodynamic Therapy of Melanoma Cells

Yifan Li¹, Yitao Fan¹, Qian Liu², Xuya Wang², Yuxia Jin², Muzhou Teng*^{1,2}

1. Department of Dermatology, The Second Hospital & Clinical Medical School, Lanzhou University, Lanzhou, China.
2. Gansu Provincial Maternity and Child-Care Hospital (Gansu Provincial Central Hospital), Lanzhou, China.

Corresponding author: Prof. Muzhou Teng (smutmz@126.com)

Abstract

Photodynamic therapy (PDT) has emerged as a promising anticancer strategy due to its non-invasive nature and precise spatiotemporal control. However, conventional photosensitizers (PSs) suffer from aggregation-caused quenching (ACQ), poor hydrophilicity, and serious oxygen dependence, limiting their clinical utility. To address these challenges, we developed an efficient strategy to fabricate hydrophilic aggregation-induced emission (AIE)-active Bovine Serum Albumin (BSA) Encapsulates PSs via an effective light-mediated thiol-yne click reaction. By designing alkynyl-functionalized AIE-active PSs with strong

generating capability of type I/II reactive oxygen species (ROS), we achieved fast combination with thiol-rich BSA under UV light irradiation, forming stable BSA@AIE-active PSs' nanoparticles (NPs). The resulting NPs exhibited excellent water dispersibility, bright fluorescence and intense ROS generation. *In vitro* studies demonstrated their outstanding PDT effect to melanoma cell (B16-F10) under white light irradiation. This work proposed a universal, scalable, and eco-friendly platform for constructing AIE-active hydrophilic PS's NPs, overcoming longstanding hurdles in PS's hydrophobicity and fabrication complexity.

Keywords: Aggregation-induced emission, click reaction, photodynamic therapy, bovine serum albumin, melanoma cell

Introduction

Photodynamic therapy (PDT), as a non-invasive and spatiotemporally controllable treatment technology, has attracted increasing research interests in biomedical field.^[1-3] By leveraging light-activated photosensitizers (PSs) to generate cytotoxic reactive oxygen species (ROS), PDT offers an effective approach to eliminate cancer cells while minimizing damage to healthy tissues.^[4] However, some disadvantages of conventional PSs make them difficult to achieve highly efficient practical applications, such as typical and head-scratching aggregation-caused quenching (ACQ) effect,^[5] poor water solubility, and serious oxygen

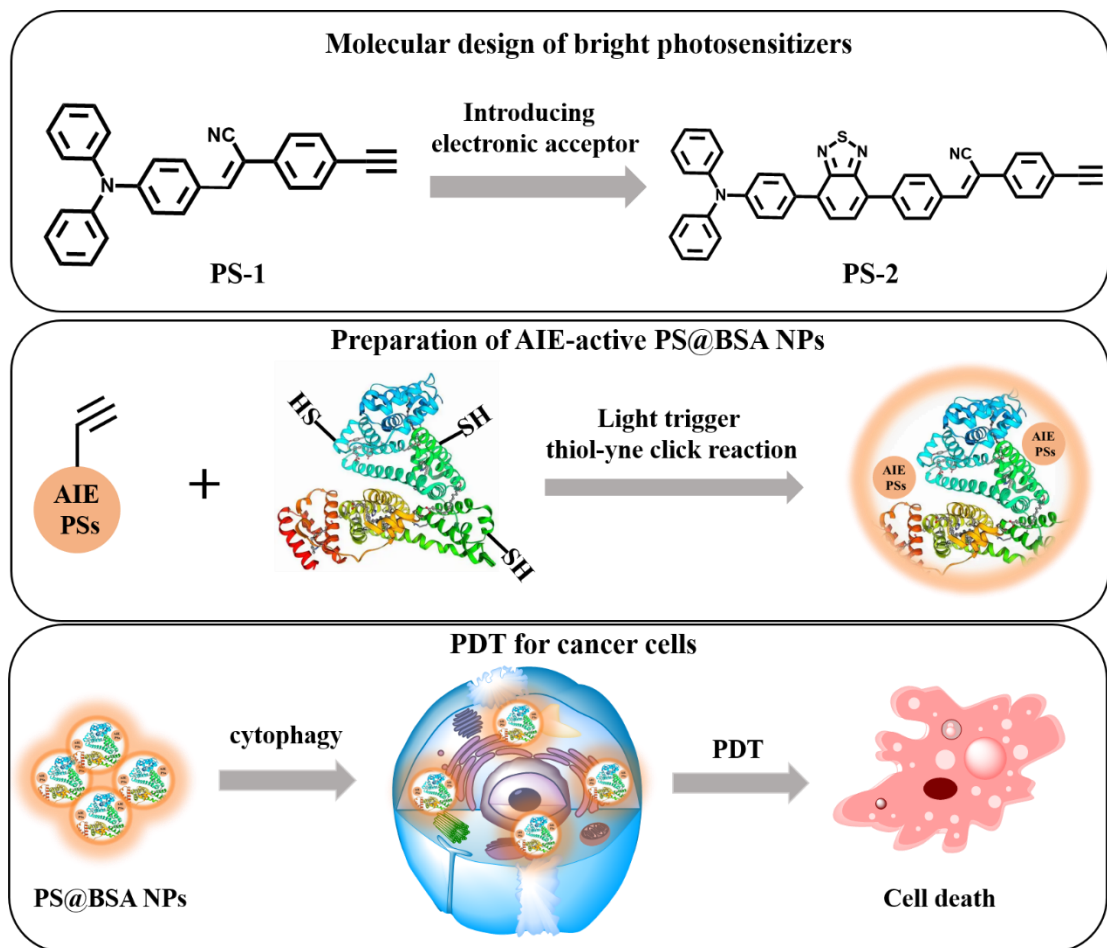
dependence.^[6] These drawbacks often lead to reduced fluorescence and ROS generation efficiency, suboptimal biocompatibility, and limited therapeutic efficiency. In recent years, aggregation-induced emission (AIE)-active PSs have emerged as a revolutionary class of photosensitizers (PSs),^[7-8] addressing effectively the ACQ problem by exhibiting enhanced luminescence and ROS generation in the aggregated state.^[9-11] Despite their a series of advantages, the hydrophobic nature of most aromatic AIE-active PSs poses challenges in achieving stable aqueous dispersion, necessitating additional chemical modifications or carrier systems to improve biocompatibility.^[12-15] This trade-off between functionality and practicality underscores the urgent need for innovative strategies to streamline the fabrication of AIE-based nanoplatforms without compromising performance.

Click chemistry, renowned for its high efficiency, selectivity, and mild reaction conditions, has become an important protocol to fabricate biomedical materials and modify surface,^[16-19] which has promising applications in the fields of bioconjugation and nanomaterial engineering. Among its diverse reactions, the light-triggered thiol-yne click reaction stands out for its spatiotemporal control and catalyst-free nature, making it particularly suitable for biomedical applications.^[20-23] By exploiting the rapid and specific coupling between alkyne and thiol groups under light irradiation, this strategy enables precise functionalization of biomolecules

while preserving their native activity. Building on this principle, we herein report a novel methodology for constructing hydrophilic AIE-active PSs' nanoparticles via a one-step photo-click reaction between alkynyl-functionalized AIE-active PSs and thiol group contained Bovine Serum Albumin (BSA). This approach not only circumvents the need for toxic catalysts but also integrates the advantages (aggregation enhances fluorescence and ROS efficiency) of AIE-active PSs with the inherent biocompatibility of BSA, yielding nanoscale PSs with superior water dispersibility, better biocompatibility and effective PDT to cancer cells.

Based on above description, in this research work, two type BSA encapsulated AIE-active PSs' nanoparticles (NPs) were designed and prepared. First, the incorporation of alkyne group into AIEgens to fabricate two donor (D)-acceptor (A) type PSs (namely as PS-1 and PS-2) by ingenious chemical synthesis. Then, BSA was used to react with above AIE-active PSs to afford AIE-active PSs' NPs via light-mediated thiol-yne click addition reaction (**Scheme 1**). The detail synthetic processes were described in the supporting information (**Figure S1**). For the molecular design, PS-2 had additional electronic acceptor of benzothiadiazole than PS-1, which was expected to achieve red fluorescence of BSA@PS NPs. Experimental result showed that resulting nanocomposites retain the AIE-active PSs' robust ROS generation capability. Systematic evaluations demonstrated that these BSA-based AIE-active PSs' NPs form small

nanoparticles with diameters of near 100 nm. *In vitro* studies further revealed their potent anticancer cells efficacy under light irradiation, achieving over 90% cancer cell ablation, alongside excellent photostability and minimal dark toxicity. This work represents an effective method in fabricating biocompatible AIE-active PS's NPs, which is expected to provide a foundational framework for the industrial-scale production of biocompatible AIE-active PSs.



Scheme 1 Demonstration of molecular structures of PSs and light trigger thiol-yne click reaction to fabricate AIE-active PS@BSA nanoparticles for photodynamic anticancer cells.

Results and discussion

Synthesis and characterization of PS-1 and PS-2

Targeted PS-1 and PS-2 were synthesized by combining typical chemical reaction of Suzuki reaction and Knoevenagel condensation reaction, which was purified by the filtration and wash for three times by using heated ethanol with a better yields of 83% and 72%. Firstly, molecular structure of PS-1 was constructed by adopting triphenylamine (TPA) as electronic donor and phenylacetonitrile as electronic acceptor. Differently, PS-2 had additional electronic acceptor of benzothiadiazole than PS-1, which was expected to redshift maximal fluorescence peak.^[24] Chemical structures of intermediate and final products were clearly characterized by hydrogen/carbon nuclear magnetic resonance ($^1\text{H}/^{13}\text{C}$ NMR) and high-resolution mass spectra (**Figure S2-8**).

Photophysical properties and theoretical calculation

The photophysical properties of PS-1 and PS-2 were initially evaluated (**Figure 1A**). Both compounds demonstrated good solubility in tetrahydrofuran (THF), with absorption maxima observed at 405 nm and 495 nm, respectively. Their photoluminescence (PL) spectra with maximal emissive wavelength peaked at 557 nm and 629 nm, respectively. Therefore, photophysical property of absorption and fluorescent spectra suggested that PS-1 emitted yellow fluorescence and PS-2 emitted red fluorescence, ascribed to the enhanced intramolecular charge transfer (ICT) effect after inserting electronic acceptor of benzothiadiazole in the PS-2.^[25-26] Notably, PS-1 achieved a significantly higher photoluminescence

quantum yield (32.7%) in neat film compared to PS-2 (11.4%), it might be contributed to the intramolecular charge transfer (ICT) effect quenched fluorescence.^[27] In addition to this reason, different molecular packing modes of these two emitters might cause the difference on their photoluminescence quantum yields.^[28-29] Theoretical analyses of frontier molecular orbital distributions revealed electron transition process (**Figure 1B**). For the highest occupied molecular orbital (HOMO) of PS-1, electron density localized predominantly on the triphenylamine unit, while the electron of the lowest unoccupied molecular orbital (LUMO) concentrated at phenylacetonitrile unit. Differently, electrons of HOMO of PS-2 distributed on the units of triphenylamine and benzothiadiazole, while the LUMO's electrons also concentrated at benzothiadiazole and phenylacetonitrile unit. Theoretical calculation of transition decay was carried out, PS-1 and PS-2 had the transition decay of 4.63 Debye and 5.71 Debye, the larger transition decay of PS-2 was well match with its longer absorption and emissive wavelength.

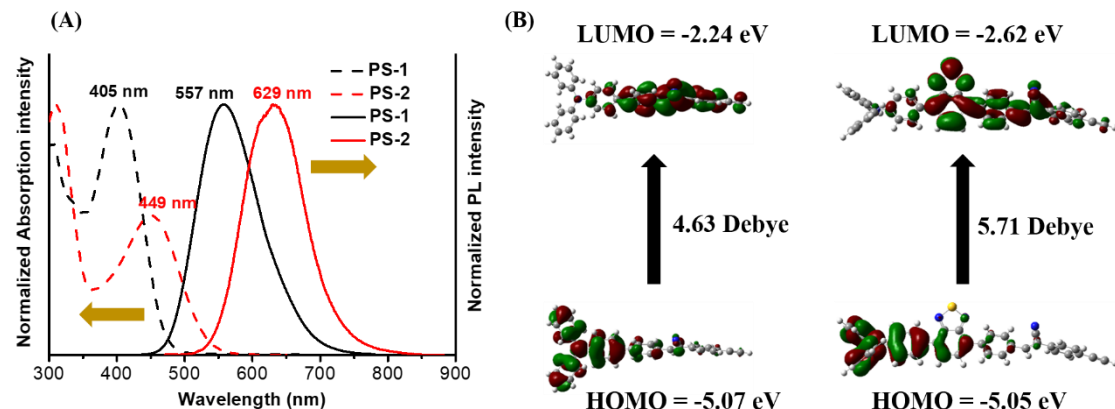


Figure 1 (A) UV-vis absorption and PL spectra of PS-1 and PS-2 in THF solvent; (B)

Electron distribution of HOMOs/LUMOs and their calculated values based on b3lyp/6-31g(d,p). [PS-1] = 10 μ M, [PS-2] = 10 μ M.

To explore the correlation between solvent polarity and emitter's fluorescence, ultraviolet visible (UV-vis) absorption and photoluminescence spectra of the two emitters were recorded in different organic solvents with different polarity. Absorption spectra showed small maximal spectral shift accompanying with increased solvent polarity (**Figure 2A-B**), indicating negligible solvatochromic effect of ground-state electronic structure to environmental polarity. Oppositely, excited-state property displayed obvious polarity-dependent trend, evidenced by progressive emission redshift and fluorescence attenuation across the solvent gradient (**Figure 2C-D**). PS-1 exhibited a bathochromic displacement from 493 nm in hexane to 634 nm in dimethyl sulfoxide (DMSO), while PS-2 manifested analogous solvatochromic behavior, shifting from 538 nm to 674 nm under same condition (**Figure 2E-F**). This pronounced excited-state sensitivity stemmed from polar media-induced stabilization of ICT state, as supported by spectral progression trend.^[30] The solvent-dependent spectral alterations conclusively validate strong ICT attributes in both emitters, with solvation effects preferentially stabilizing charge-separated excited-state configurations in highly polar environments.

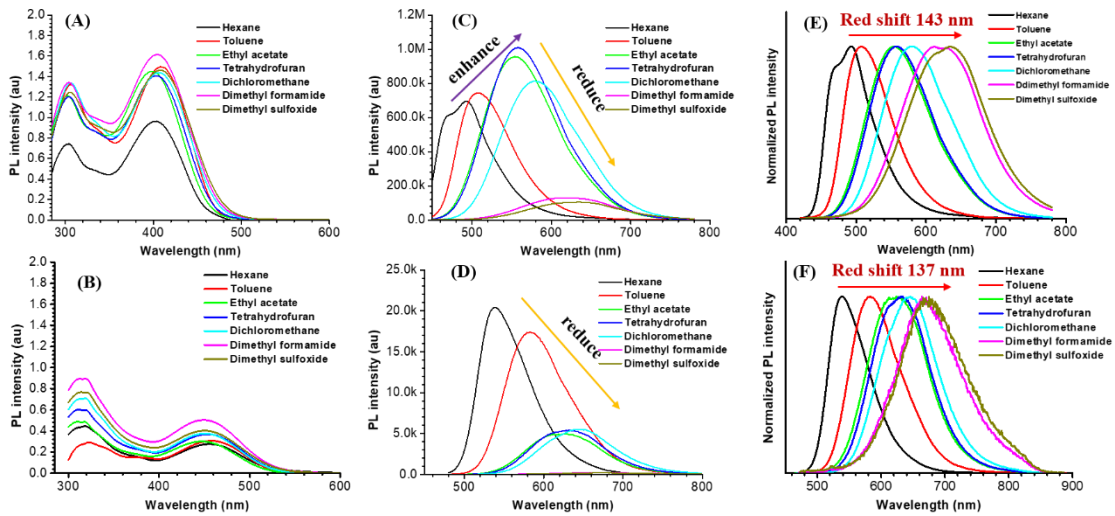


Figure 2 Absorption spectra of PS-1 (A) and PS-2 (B) in different organic solvents; PL spectra of PS-1 (C) and PS-2 (D) in different organic solvents; Normalized PL spectra of PS-1 (E) and PS-2 (F) in different organic solvents. Concentration: 20 μ M.

AIE property of both emitters were systematically evaluated. Firstly, the PLQYs of these two emitters in DMSO and neat film were measured. the PLQYs of PS-1 and PS-2 were detected as 22.5% and 18.9% in DMSO. In neat film, the PLQYs of PS-1 and PS-2 were 32.7% and 11.4%, above results suggested preliminarily that PS-1 had aggregation enhanced emission (AEE) nature, but PS-2 might show aggregation caused fluorescence quench effect. To further confirm their AIE property, as depicted in **Figure 3A-B**, their PL spectra displayed distinct emission trends in DMSO/H₂O mixture with incremental aqueous content. In pure DMSO, the emitters exhibited orange fluorescence, contrasting sharply with classical AIE luminogens (AIEgens) like tetraphenylethylene (TPE) and hexaphenylsilole (HPS),^[31-32] where dissolved in good solvents typically exhibited very weak fluorescence. For the PS-1, when increasing the water fraction to 60%, fluorescence intensity enhanced progressively

alongside a 76 nm blue shift in maximal emission peak. The improved fluorescent intensity was contributed to the AIE effect, while blue shift of maximal emissive peak within 60% water fraction could be attributed to the changed polar environment from high-polarity DMSO solvent to low-polarity aggregates. Similarly, PS-2 also showed that the fluorescence intensity decreased first and then increased, which was contributed to the synergistic effect of “AIE+TICT”.^[33]

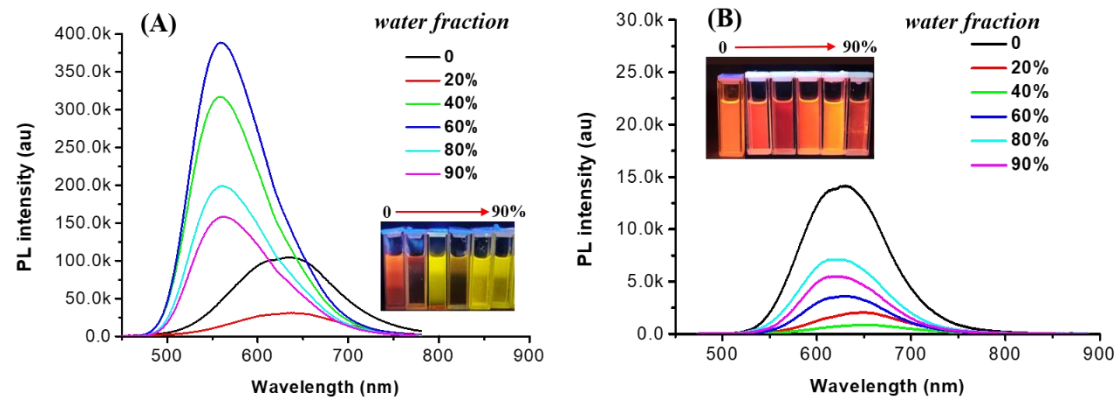


Figure 3 Fluorescent spectra of PS-1 (A) and PS-2 (B) in DMSO/H₂O mixture solvents with different water fraction. Concentration: 20 μM.

Detection of reactive oxygen species

PDT functions as a non-invasive therapeutic approach that leverages light-activated PSs to generate cytotoxic ROS. This mechanism relies on biocompatible PSs absorbing visible light to generate triplet excited states, which then facilitates energy and electron transfer to molecular oxygen. To quantitatively assess ROS production in PS-1 and PS-2, we utilized DCFH dye, a fluorescent probe emitting at maximal 524 nm upon oxidation by ROS. Both PSs demonstrated efficient ROS generation under white light irradiation, consistent with their strong visible-light absorption capability.

Control experiments (**Figure S9A**) revealed minimal background fluorescence from 2',7'-dichlorofluorescein diethylenetriacetate (DCFH-DA) alone under illumination. In contrast, solutions containing PS-1 and PS-2 exhibited substantial fluorescence enhancement upon light exposure (**Figure 4A** and **Figure S9B-C**). Comparative analysis of fluorescent intensity amplification conclusively identified PS-1 as the superior ROS generator under same irradiation condition, achieving markedly higher efficiency than PS-2.

Photodynamic activity generally proceeds through two distinct routes for ROS production: (1) energy transfer from the triplet-excited state of PSs to molecular oxygen, producing singlet oxygen (${}^1\text{O}_2$), (2) electron transfer reactions that generate superoxide radicals (O_2^-) and hydroxyl radicals ($\cdot\text{OH}$).^[34] To determine the predominant ROS species generated by PS-1 and PS-2, we utilized the selective ${}^1\text{O}_2$ probe of 9,10-anthracenediyl-bis(methylene)-dimalonic acid (ABDA). The anthracene-based compound ABDA specifically reacts with ${}^1\text{O}_2$ through irreversible endoperoxide formation, enabling quantification via absorbance loss at characteristic wavelengths. Initial control measurement showed negligible absorbance changes in only ABDA solution under prolonged white-light illumination (**Figure 4B** and **Figure S10**). However, systems incorporating PS-1 or PS-2 exhibited marked absorbance reduction, confirming effective ${}^1\text{O}_2$ generation by both PSs. Comparative analysis revealed PS-1 induced

significantly greater ABDA degradation than PS-2, establishing its superior ${}^1\text{O}_2$ production capability under equivalent irradiation conditions.

The generation of type I ROS, specifically O_2^- and $\cdot\text{OH}$, was systematically investigated using fluorescent probes of dihydrorhodamine 123 (DHR123) and hydroxyphenyl fluorescein (HPF).^[35] Initial verification of O_2^- production was conducted through DHR123, a non-fluorescent compound that exhibits distinct green fluorescence emission at 525 nm upon interaction with O_2^- . As demonstrated in **Figure 4C** and **Figure S11**, control experiment revealed minimal fluorescence variation in pure DHR123 solutions under 5-minute irradiation. However, significant fluorescence enhancement was observed when PS-1 or PS-2 solution containing DHR123 were exposed to white light, confirming effective O_2^- generation. Subsequent $\cdot\text{OH}$ detection using hydroxyphenyl fluorescein (HPF) probe showed differential radical production between compounds. **Figure 4D** and **Figure S12** illustrated that the PS-2 and HPF combination exhibited stronger fluorescence intensity compared to PS-2 and HPF combination, indicating superior $\cdot\text{OH}$ generation efficiency in PS-2. Therefore, according to above analysis, PS-1 has better O_2^- and ${}^1\text{O}_2$ generation, while PS-2 shows more efficient $\cdot\text{OH}$ generation than PS-1.

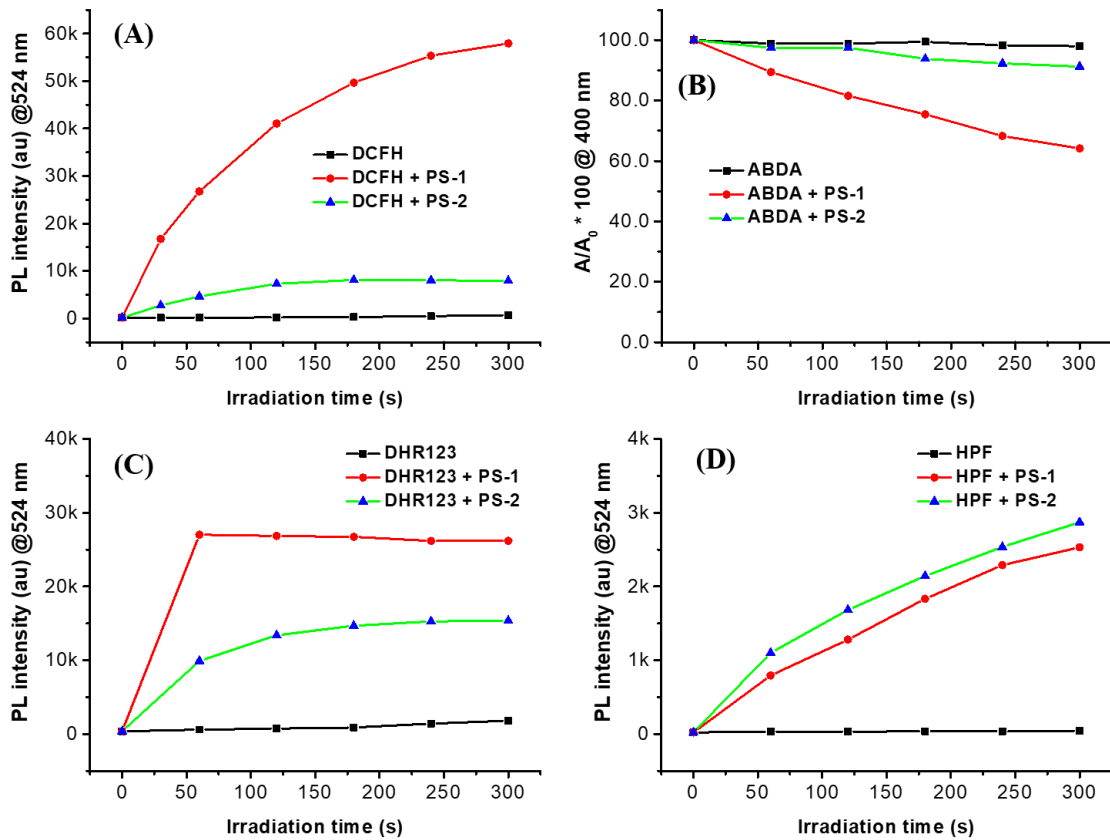


Figure 4. (A) Measurement of total ROS of PS-1 (5 μ M) and PS-2 (5 μ M) by using DCFH (10 μ M) probe upon white light irradiation, (B) access of $^1\text{O}_2$ generation with the decomposition of ABDA (20 μ M) probe after mixing PS-1 (5 μ M) and PS-2 (5 μ M) upon white light irradiation, (C) access of O_2^- generation of PS-1 (2 μ M) and PS-2 (2 μ M) by using DHR123 (10 μ M) probe upon white light irradiation, (D) access of $\cdot\text{OH}$ generation of PS-1 (2 μ M) and PS-2 (2 μ M) by using HPF (10 μ M) probe upon white light irradiation, white light power: 30 mW/cm².

PDT effect of B16-F10 cancer cells

Due to the favorable ROS generation and fluorescence efficiency of PS-1 and PS-2, their PDT potential was assessed at the cellular level by choosing B16-F10 cancer cells as research object. However, both PSs exhibited pronounced hydrophobicity, hindering cellular uptake. To address this limitation, the natural polymer of BSA was employed to link covalently with PSs to enhance their hydrophilicity because alkynyl of PSs could happen click reaction with thiol group of BSA, therefore yielding stable PS-

1@BSA NPs and PS-2@BSA NPs with enhanced aqueous dispersibility. Dynamic light scattering (**Figure S13A-B**) revealed hydrodynamic diameters of near 100 nm for PS-1@BSA NPs and PS-2@BSA NPs, with nanoscale dimensions promoting efficient cellular uptake. Their zeta potentials were measured as -36.43 mV and -37.03 mV, and the encapsulation efficiency of PS-1@BSA NPs and PS-2@BSA NPs are about 25.0% and 34.7%. Furthermore, two NPs have better photostability after frequent irradiation by UV light because of not obvious reduction of absorption intensity (**Figure S14**). Next, photophysical properties and ROS performance of PS-1@BSA NPs and PS-2@BSA NPs were characterized. As shown in **Figure S15**, comparing the absorption spectra of PS-1/ PS-1@BSA NPs and PS-2/ PS-2@BSA NPs, it can be known that absorption spectra of BSA-based NPs show a significant redshift phenomenon. For example, PS-1 in THF had the maximal absorption spectrum of 405 nm, but red-shifted to the 434 nm after forming PS-1@BSA NPs. PS-2@BSA NPs showed maximal absorption wavelength of 496 nm, which was larger than PS-2 in THF with maximal absorption peak of 451 nm. Oppositely, comparing with PS-1/PS-2 in THF, the maximal emissive peaks of PS-1@BSA NPs and PS-2@BSA NPs showed a slight blueshift (**Figure S16**). Probes of DHR123 and HPF were used to characterize the type I ROS generation of PS-based BSA NPs, as shown in **Figure S17-18**, fluorescent intensity from DHR123 and HPF showed obvious enhancement,

suggesting an effective generation of O_2^- and $\cdot OH$.

To evaluate intracellular ROS production, the DCFH fluorescent probe was utilized, B16-F10 cancer cells co-treated with PS@BSA NPs exhibited bright green fluorescence, confirming effective ROS generation (**Figure S19**). According to **Figure 5C-D**, cytocompatibility study demonstrated that over 95% cell viability at high PS@BSA NPs concentration (200 $\mu g/mL$), underscoring their better biocompatibility. Upon light irradiation, both PS@BSA NPs caused substantial cell death, validating their great PDT efficacy. Live/dead staining assays further corroborated effective PDT result (**Figure 5E**), that are, when B16-F10 cancer cells uptake PS-1@BSA NPs and PS-2@BSA NPs, after a period of white light irradiation, a large area of cells showed obvious red fluorescence. It was directly proved that the prepared PS-1@BSA NPs and PS-2@BSA NPs had good PDT efficacy, which is expected to show great application potential for treating cancer.

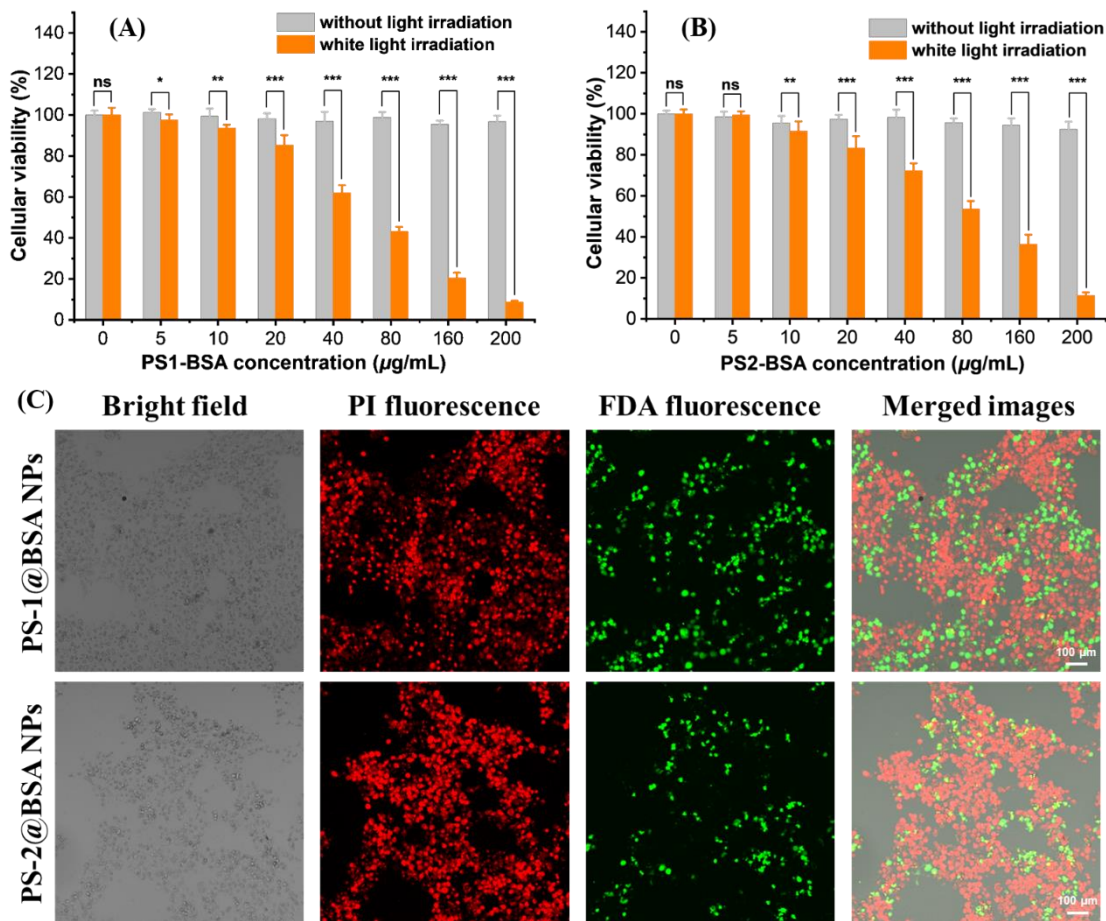


Figure 5 (A) PS-1@BSA NPs, (B) PS-2@BSA NPs against B16-F10 cancer cells at varying concentrations, (C) Live/dead cell costaining assays using FDA and Propidium iodide (PI) as fluorescence probes for PS-1@BSA NPs and PS-2@BSA NPs, scale bar: 100 μm , [PI] = 2 μM , [FDA] = 5 μM , [PS-1@BSA NPs] = 200 $\mu\text{g/mL}$, [PS-2@BSA NPs] = 200 $\mu\text{g/mL}$, white light: 30 mW cm^{-2} .

Conclusion

In summary, this work reported an effective click reaction to fabricate BSA encapsulates the AIE-active PS's NPs. Two alkynyl-contained AIE-active PSs with bright fluorescence and strong generating capability of type I/II ROS at aggregation were designed and synthesized, and their chemical structures were full confirmed by using $^1\text{H}/^{13}\text{C}$ NMR spectra and HRMS spectra. When mixing BSA and PS-1/PS-2 solution and receiving UV light irradiation, two stable PS-1@BSA NPs and PS-2@BSA NPs with

enhanced aqueous dispersibility and small size of near 100 nm were obtained, which could effectively produce type I ROS of O_2^- and $\cdot OH$, which showed good PDT efficacy to the B16-F10 cancer cells. This work proposed a universal and eco-friendly method for constructing hydrophilic AIE-active PS's NPs, which is expected to show huge promising potential for future biomedical applications.

Conflict of interest statement

There are no conflicts to declare.

Acknowledgements

This work is supported by Special fund for laboratory animals of Gansu Natural Science Foundation (24JRRA379), Foundation of Gansu Province (23JRRA1518), Provincial Talent Project of Gansu Province (GZTZ2024-4), Project of Gansu Provincial Department of Education (2023QB-056), Talent Innovation and Entrepreneurship Project of Lanzhou City (2022-RC-49), Talent Innovation and Entrepreneurship Project of Chengguan District (2022-rc-7), Scientific Research Fund Project of the Hospital(GMCCH2024-2-4).

References

- [1] Pham, T. C.; Nguyen, V.; Choi, Y.; Lee, S.; Yoon, J. Recent Strategies to Develop Innovative Photosensitizers for Enhanced Photodynamic

- Therapy. *Chem. Rev.* **2021**, *121*, 13454-13619.
- [2] Zhang, W.; Ahmed, A.; Cong, H.; Wang, S.; Shen, Y.; Yu, B. Application of multifunctional BODIPY in photodynamic therapy. *Dyes Pigments*. **2021**, *185*, 108937.
- [3] Algorri, J. F.; Ochoa, M.; Roldán-Varona, P.; Rodríguez-Cobo, L.; López-Higuera, J. M. In *Cancers*, 2021; Vol. 13.
- [4] Tao, T.; Hu, X.; Sun, D.; Ou, C.; Guo, Y.; Xu, H. The halogen effect of bis-truxene substituted BODIPY photosensitizers for potential photodynamic therapy. *Dyes Pigments*. **2024**, *224*, 111996.
- [5] Yu, Y.; Jia, H.; Liu, Y.; Zhang, L.; Feng, G.; Tang, B. Z. Recent Progress in Type I Aggregation-Induced Emission Photosensitizers for Photodynamic Therapy. *Molecules*, **2023**, *28*, 332.
- [6] Ni, J.; Wang, Y.; Zhang, H.; Sun, J. Z.; Tang, B. Z. Aggregation-Induced Generation of Reactive Oxygen Species: Mechanism and Photosensitizer Construction. *Molecules*, **2021**, *26*, 268.
- [7] Wang, X.; Yang, L.; Li, Y. H.; Wang, X. H.; Qi, Z. J. A Long-Retention Cell Membrane-Targeting AIEgen for Boosting Tumor Theranostics. *Chem-AsianJ.* **2024**, *19*, e202400305.
- [8] Wang, X.; Tang, Y. Q.; Liang, J. K.; Zhao, Y. F.; Yang, L.; Qi, Z. J. A lipid droplet-specific near-infrared automatic oxygen-supplied AIEgen for photodynamic therapy and metastasis inhibition of hypoxic tumors. *Chem. Eng. J.* **2023**, *453*, 139838.

- [9] Gao, J.; Tian, Y.; Li, Y.; Hu, F.; Wu, W. Design strategies for aggregation-induced emission photosensitizers with enhanced safety in photodynamic therapy. *Coord. Chem. Rev.* **2024**, *507*, 215756.
- [10] Wan, Q.; Li, Y.; Ding, K.; Xie, Y.; Fan, J.; Tong, J.; Zeng, Z.; Li, Y.; Zhao, C.; Wang, Z. et al. Aggregation Effect on Multiperformance Improvement in Aryl-Armed Phenazine-Based Emitters. *J. Am. Chem. Soc.* **2023**, *145*, 1607-1616.
- [11] Li, Y.; He, D.; Wan, Q.; Tang, B. Z.; Wang, Z. An innovative stepwise activated coupling reaction for fabricating functional fluorescence probes with potential photosensitive applications. *Sensor Actuator B-Chem.* **2024**, *412*, 135725.
- [12] Wang, X.; Li, Y. H.; Hasrat, K.; Yang, L.; Qi, Z. J. Sequence-Responsive Multifunctional Supramolecular Nanomicelles Act on the Regression of TNBC and Its Lung Metastasis via Synergic Pyroptosis-Mediated Immune Activation. *Small*, **2023**, *19*, 2305101.
- [13] Wang, X.; Li, Y. H.; Qi, Z. J. Light-Enhanced Tandem-Responsive Nano Delivery Platform for Amplified Anti-tumor Efficiency. *Chem-AsianJ.* **2024**, *19*, e202400311.
- [14] Zheng, Y.; Li, Y.; Bai, X.; Teng, M.; Tang, Y.; Zhao, S.; Ma, Z.; Liang, H.; Xie, Y.; Wan, Q. Atomic Engineering and Aggregation Effect to Regulate Synergistically Type I Reactive Oxygen Species of AIE-Active Deep Red/Near Infrared Red Photosensitizer. *Small* **2025**, *21*, 2410816.

- [15] Min, X.; Yi, F.; Han, X.; Li, M.; Gao, Q.; Liang, X.; Chen, Z.; Sun, Y.; Liu, Y. Targeted photodynamic therapy using a water-soluble aggregation-Induced emission photosensitizer activated by an acidic tumor microenvironment. *Chem. Eng. J.* **2022**, *432*, 134327.
- [16] Li, X.; Xiong, Y. Application of “Click” Chemistry in Biomedical Hydrogels. *ACS Omega* **2022**, *7*, 36918-36928.
- [17] Kaur, J.; Saxena, M.; Rishi, N. An Overview of Recent Advances in Biomedical Applications of Click Chemistry. *Bioconjug. Chem.* **2021**, *32*, 1455-1471.
- [18] Albada, B.; Keijzer, J. F.; Zuilhof, H.; van Delft, F. Oxidation-Induced “One-Pot” Click Chemistry. *Chem. Rev.* **2021**, *121*, 7032-7058.
- [19] McDaniel, R. M.; Carey, M. S.; Wilson, O. R.; Barsoum, M. W.; Magenau, A. J. D. Well-Dispersed Nanocomposites Using Covalently Modified, Multilayer, 2D Titanium Carbide (MXene) and In-Situ “Click” Polymerization. *Chem. Mat.* **2021**, *33*, 1648-1656.
- [20] Sradha S, A.; Sariga; George, L.; Varghese, A. Advancements in thiol-yne click chemistry: Recent trends and applications in polymer synthesis and functionalization. *Mater. Today Chem.* **2024**, *38*, 102112.
- [21] Lü, S.; Wang, Z.; Zhu, S. Thiol-Yne click chemistry of acetylene-enabled macrocyclization. *Nat. Commun.* **2022**, *13*, 5001.
- [22] Wang, B.; Li, C.; He, D.; Ding, K.; Tian, Q.; Feng, G.; Qin, A.; Tang, B. Z. Bioconjugation and Reaction-Induced Tumor Therapy via

- Alkynamide-Based Thiol-Yne Click Reaction. *Small* **2024**, *20*, 2307309.
- [23] Mitmoen, M.; Kedem, O. UV- and Visible-Light Photopatterning of Molecular Gradients Using the Thiol–yne Click Reaction. *ACS Appl. Mater. Interfaces* **2022**, *14*, 32696-32705.
- [24] Deng, D.; Yang, Y.; Liu, S.; Deng, X.; Chen, Z.; Pu, S. Benzothiadiazole-based dibenzobenzimidazole derivatives with aggregation-induced deep-red fluorescence and different mechanically responsive fluorescence features. *Dyes Pigments*. **2022**, *205*, 110580.
- [25] He, Y.; Xie, F.; Li, H.; Zhang, K.; Shen, Y.; Ding, F.; Wang, C.; Li, Y.; Tang, J. Red-shift emission and rapid up-conversion of B,N-containing electroluminescent materials via tuning intramolecular charge transfer. *Mater. Chem. Front.* **2023**, *7*, 2454-2463.
- [26] Long, J.; Shan, J.; Zhao, Y.; Ji, Y.; Tan, H.; Wang, H. Dramatically Enhanced and Red-shifted Photoluminescence Achieved by Introducing an Electron-withdrawing Group into a Non-traditional Luminescent Small Organic Compound. *Chem-Asian J.* **2021**, *16*, 2426-2430.
- [27] Wu, H.; Du, L.; Luo, J.; Wang, Z.; Phillips, D. L.; Qin, A.; Tang, B. Z. Structural modification on tetraphenylpyrazine: from polarity enhanced emission to polarity quenching emission and its intramolecular charge transfer mechanism. *J. Mater. Chem. C* **2022**, *10*, 8174-8180.
- [28] Wang, J. F.; Cao, M. Y.; Han, L. L.; Shangguan, P.; Liu, Y. S.; Zhong, Y.; Chen, C. Y.; Wang, G. Y.; Chen, X. Y.; Lin, M.; Lu, M. Y.; Luo, Z. Q.;

He, M.; Sung, H. H. Y.; Niu, G. L.; Lam, J. W. Y.; Shi, B. Y.; Tang, B. Z. Blood–Brain Barrier-Penetrative Fluorescent Anticancer Agents Triggering Paraptosis and Ferroptosis for Glioblastoma Therapy, *J. Am. Chem. Soc.* **2024**, *146*, 42, 28783–28794.

[29] Cao, S. X.; Tian, X. Y.; Cao, M. Y.; Wang, J. G.; Niu, G. L.; Tang, B. Z. Solvatochromic Near-Infrared Aggregation-Induced Emission-Active Acrylonitriles by Acceptor Modulation for Low-Power Stimulated Emission Depletion Nanoscopy, *Chem. Mater.* **2023**, *35*, 6, 2472–2485.

[30] Wan, Q.; Dai, W.; Xie, Y.; Ke, Q.; Zhao, C.; Zhang, B.; Zeng, Z.; Wang, Z.; Tang, B. Z. AIE-active deep red/near-infrared electroluminescent emitters with fine regulation of excited state. *Chem. Eng. J.* **2023**, *451*, 138529.

[31] Li, D.; Zuo, R.; Wang, J.; Le, Z. The Designs and Applications of Tetraphenylethylene Macrocycles and Cages. *Chem-Eur J.* **2025**, *31*, e202403715.

[32] Ito, F. Fluorescence Detection of Dynamic Aggregation Processes Using AIEgens, 2022.

[33] Huang, J.; Zhou, Y.; Wang, W.; Zhu, J.; Li, X.; Fang, M.; Wu, Z.; Zhu, W.; Li, C. A fluorescent probe based on triphenylamine with AIE and ICT characteristics for hydrazine detection. *Spectrochimica Acta Part a: Molecular and Biomolecular Spectroscopy* **2023**, *286*, 122011.

[34] Tang, Y.; Xie, Y.; Bai, X.; Zhao, C.; Zheng, Y.; Liang, H.; Ma, Z.;

Wang, Z.; Wan, Q. Building Block for Designing Bright Type I AIE-Active Photosensitizers with Deep/Near-infrared Red Fluorescence. *Chemistry – an Asian Journal* **2025**, *20*, e202401276.

[35] Wan, Q.; Zhang, R.; Zhuang, Z.; Li, Y.; Huang, Y.; Wang, Z.; Zhang, W.; Hou, J.; Tang, B. Z. Molecular Engineering to Boost AIE-Active Free Radical Photogenerators and Enable High-Performance Photodynamic Therapy under Hypoxia. *Adv. Funct. Mater.* **2020**, *30*, 2002057.

Highlights:

Two bright AIE-active photosensitizers (PSs) with alkyne group could overcome the problem of conventional aggregation caused fluorescence quenching.

Thiol-yne click reaction was used to prepare biocompatible PS@BSA nanoparticles with better water dispersibility and small nanoscale size.

PS@BSA nanoparticles achieved great photodynamic therapy effect for the B16-F10 cancer cells because of effective generation of $O_2^{-\cdot}$ and $\cdot OH$.

The universal and eco-friendly method was proposed to prepare hydrophilic AIE-active PS's NPs.

Graphical Abstract

This work proposed a universal and eco-friendly light trigger thiol-yno click reaction method for preparing hydrophilic AIE-active photosensitizer's nanoparticles, which achieved great photodynamic therapy effect for the B16-F10 cancer cells.

*Supporting information***Title: Light-Triggered Click Reaction to Fabricate Bright Bovine Serum Albumin Encapsulates Photosensitizer's Nanoparticles for Effective Photodynamic Therapy of Melanoma Cells**

Yifan Li¹, Yitao Fan¹, Qian Liu², Xuya Wang², Yuxia Jin², Muzhou Teng*^{1,2}

1. Department of Dermatology, The Second Hospital & Clinical Medical School, Lanzhou University, Lanzhou, China.

2. Gansu Provincial Maternity and Child-Care Hospital (Gansu Provincial Central Hospital), Lanzhou, China.

Materials and synthesis**Materials and measurements**

All the chemical agents contained 4-Formylphenylboronic acid, 4,7-Dibromo-2,1,3-benzothiadiazole, 4-(Diphenylamino)phenylboronic acid, 4-Ethynylphenylacetonitrile, Tetrakis(triphenylphosphine)palladium ($Pd(PPh_3)_4$), Tetramethylammonium hydroxide (TBAH), potassium carbonate and anhydrous ethanol were purchased from commercial sources (Energy Chemical Company) and directly used without further purification.

Intermediate of TBZ-PhCHO was synthesized according to previous

reported literature.¹ ¹H and ¹³C NMR spectra were measured on a Bruker AV 500 spectrometer in *d*6-DMSO at room temperature. UV-vis absorption spectrum was measured on a Shimadzu UV-2600 spectrophotometer. PL spectra were recorded on a Horiba Fluoromax-4 spectrofluorometer. Fluorescence quantum yields were measured using a Hamamatsu absolute PL quantum yield spectrometer C11347 Quantaurus_QY.

Synthesis of TPA-PhCHO

The intermediate product of TPA-PhCHO was prepared by using 4-Bromotriphenylamine and 4-Formylphenylboronic acid as raw materials based on Suzuki reaction. 4-Bromotriphenylamine (5 mmol, 1.61 g), 4-Formylphenylboronic acid (6 mmol, 900 mg) and tetrtriphenylphosphine palladium (0.05 mmol, 58 mg) were put into the two-neck flask. Pumping and filling with N₂ for three times, THF (40 mL) and K₂CO₃ aqueous solution (2 M, 12 mL) without oxygen was injected into the flask. The reaction refluxed overnight. When the temperature cooled down, the mixture was extracted with dichloromethane for three times, the pale green powder TPA-PhCHO (1.58 g) could be obtained via the column chromatography process by using the mixture of ethyl acetate and petroleum ether as eluent, yield 91%: ¹H NMR (500 MHz, *d*6-DMSO) δ = 10.08 (s, 1H), 8.02 (d, *J* = 10 Hz, 2H), 7.93 (d, *J* = 10 Hz, 2H), 7.77 (d, *J* = 10 Hz, 2H), 7.42-7.39 (t, *J* = 15 Hz, 4H), 7.18-7.08 (m, 8H).

Synthesis of PS-1

The final product of PS-1 was prepared by using TPA-PhCHO and 4-Ethynylphenylacetonitrile as raw materials based on Knoevenagel condensation reaction. TPA-PhCHO (1 mmol, 349 mg), 4-Ethynylphenylacetonitrile (1.5 mmol, 212 mg) were put into the two-neck flask. Pumping and filling with N₂ for three times, anhydrous ethanol (20 mL) and TBAH (50 μL) without oxygen was injected into the flask. The reaction refluxed overnight. When the temperature cooled down, a large amount of powder precipitates out, which further carried out suction filtration, and the filter residue was washed with heated ethanol for three times, the yellow powder PS-1 (391 mg) was obtained, yield 83%: ¹H NMR (500 MHz, *d*6-DMSO) δ = 8.15 (s, 1H), 8.05 (d, *J* = 5 Hz, 2H), 7.86-7.80 (m, 4H), 7.73-7.663 (m, 4H), 7.37-7.34 (t, *J* = 15 Hz, 4H), 7.12-7.04 (m, 8H), 4.39 (s, 1H). ¹³C NMR (126 MHz, *d*6-DMSO) δ 147.99, 147.31, 143.61, 142.24, 132.93, 130.15, 128.24, 126.85, 126.39, 124.99, 124.06, 108.98, 83.43, 83.10. HRMS (ESI): m/z calcd. for C₃₅H₂₄N₂ = 472.1939, found m/z = 472.1926.

Synthesis of PS-2

The final product of PS-1 was prepared by using TBZ-PhCHO and 4-Ethynylphenylacetonitrile as raw materials based on Knoevenagel condensation reaction. TBZ-PhCHO (1 mmol, 483 mg), 4-Ethynylphenylacetonitrile (1.5 mmol, 212 mg) were put into the two-neck flask. Pumping and filling with N₂ for three times, anhydrous ethanol (20

mL) and TBAH (50 μ L) without oxygen was injected into the flask. The reaction refluxed overnight. When the temperature cooled down, a large amount of powder precipitates out, which further carried out suction filtration, and the filter residue was washed with heated ethanol for three times, the red powder PS-2 (436 mg) was obtained, yield 72%: ^1H NMR (500 MHz, *d*6-DMSO) δ = 8.20-8.17 (d, 3H), 7.94-7.88 (m, 5H), 7.70-7.66 (m, 5H), 7.33 (d, 4H), 7.20 (d, 6H), 7.10 (d, 2H), 5.42 (s, 1H). ^{13}C NMR (126 MHz, *d*6-DMSO) δ 153.72, 148.12, 147.25, 143.01, 135.92, 133.31, 130.69, 130.13, 130.08, 129.83, 127.64, 125.04, 124.10, 122.52, 107.51, 86.27. HRMS (ESI): m/z calcd. for $\text{C}_{41}\text{H}_{26}\text{N}_4\text{S}^+ \text{Na}^+$ = 629.1770, found m/z = 629.1780.

Click reaction between BSA and PS-1/PS-2

PS1 or PS2 (10 mg) was dissolved in tetrahydrofuran (THF) solvent (5 mL), and BSA (100 mg) was dissolved in aqueous solution (5 mL). After then, PS-contained THF solution was mixed with BSA aqueous solution, and received irradiation with ultraviolet light (365 nm) for 2 h. Finally, PS@BSA aqueous solution could be obtained after extraction by using dichloromethane and water mixture because PS@BSA product could dissolve in water, while residual PS could be removed through the extraction.

The total ROS detection by DCFH probe

The total ROS production can be monitored using DCFH as a fluorescent

probe. Aqueous solutions containing PS (5 μ M) and DCFH (20 μ M) were prepared for detection. The reaction system was illuminated with white light irradiation (30 mW/cm²), while fluorescence intensity variations at 524 nm were recorded periodically using a fluorescence spectrophotometer. Temporal changes in the fluorescence intensity were collected through continuous measurements at designated time intervals.

The $^1\text{O}_2$ detection by ABDA probe

ABDA serves as an effective probe for detecting $^1\text{O}_2$ production. An aqueous solution containing PS (5 μ M) and ABDA (20 μ M) was prepared for analysis. The sample was exposed to white light irradiation (30 mW/cm²), and UV absorption changes of ABDA at 400 nm were systematically monitored over time using a UV-Vis spectrophotometer. Kinetic analysis of $^1\text{O}_2$ generation was performed by measuring absorption variations at specific time intervals.

The O_2^- detection by DHR123 probe

The O_2^- production can be monitored using DHR123 as a fluorescent probe. Aqueous solutions containing PS (2 μ M) and DHR123 (10 μ M) were prepared for detection. The reaction system was illuminated with white light irradiation (30 mW/cm²), while fluorescence intensity variations at 524 nm were recorded periodically using a fluorescence spectrophotometer. Temporal changes in the fluorescence intensity were collected through continuous measurements at designated time intervals.

The hydroxyl radical ($\cdot\text{OH}$) detection by HPF

The $\cdot\text{OH}$ production can be monitored using HPF as a fluorescent probe. Aqueous solutions containing PS (2 μM) and HPF (10 μM) were prepared for detection. The reaction system was illuminated with white light irradiation (30 mW/cm²), while fluorescence intensity variations at 524 nm were recorded periodically using a fluorescence spectrophotometer. Temporal changes in the fluorescence intensity were collected through continuous measurements at designated time intervals.

5. Cell Culture

B16-F10 cancer cells were cultured in Dulbecco's modified Eagle's medium (DMEM) containing 10% fetal bovine serum at 37 °C in a humidified environment containing 5% CO₂.

Cell Cytotoxicity Studies

B16-F10 cancer cells were plated in 96-well plates at a density of 8×10^4 cells/mL. After allowing 12 hours for cell adhesion, varying concentrations of PS@BSA NPs were introduced and incubated under dark conditions at 37°C for 8 hours. Following thorough PBS washes to remove unbound NPs, the cells were divided into two experimental groups: one shielded from light and the other exposed to white light irradiation (30 mW/cm², 30 minutes). Both groups were subsequently incubated for an additional 18 hours at 37°C. After aspirating the supernatant, freshly prepared CCK-8 solution was added to each well. Cellular metabolic activity was quantified

by measuring absorbance at 450 nm using a microplate reader after a 4-hour incubation period with the reagent.

Intracellular ROS production imaging

B16-F10 cancer cells were seeded into confocal-compatible culture dishes at a density of 2×10^5 cells/mL and allowed to adhere for 12 hours. The adherent cells were then treated with PS@BSA NPs (200 $\mu\text{g}/\text{mL}$) for 8 hours. Following thorough PBS washes to remove unbound NPs, the cells underwent a 12-hour incubation period. Intracellular ROS detection was initiated by exposing the cells to DCFH (10 μM) for 30 minutes. After additional PBS washes, the cells were maintained in DMEM medium and subjected to white light irradiation (30 mW/cm^2) for varying durations. ROS generation was dynamically monitored via confocal microscopy, with fluorescence signals corresponding to ROS levels captured at specified time intervals.

Cell apoptosis imaging

After B16-F10 cancer cells were incubated with NPs for 8 h, then cells were washed with PBS twice. After that, these cells were treated upon white laser (30 mW/cm^2) irradiation for 10 min. 18 h later, the cells were then incubated with FDA (2 μM) and PI (4 μM) for 30 min. After washing, the cells were imaged by a confocal microscope.

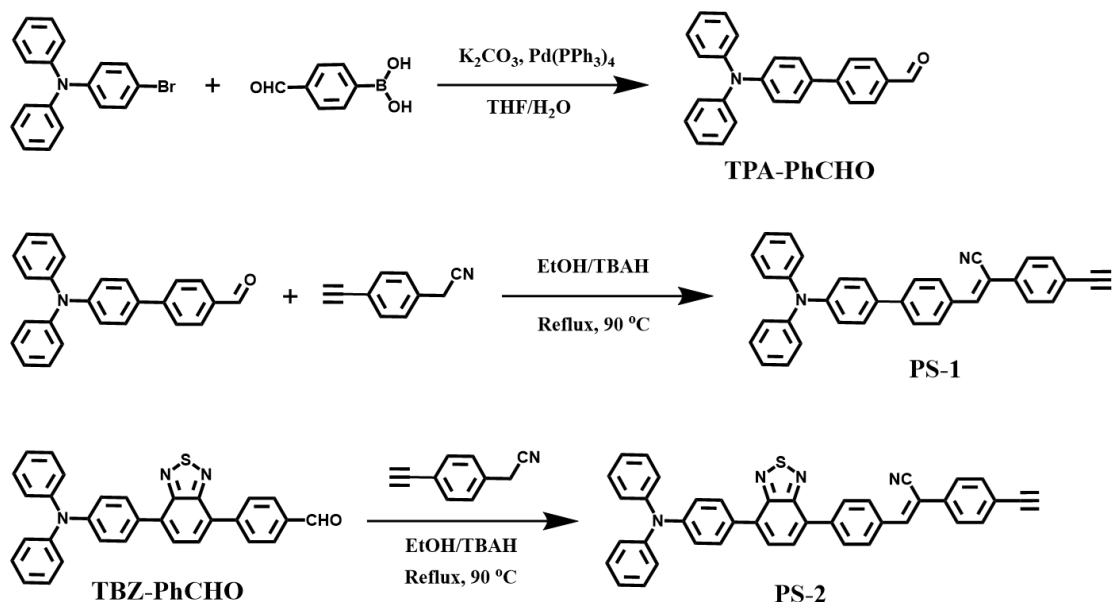


Figure S1 Synthetic routes of intermediate and targeted products of PS1 and PS2.

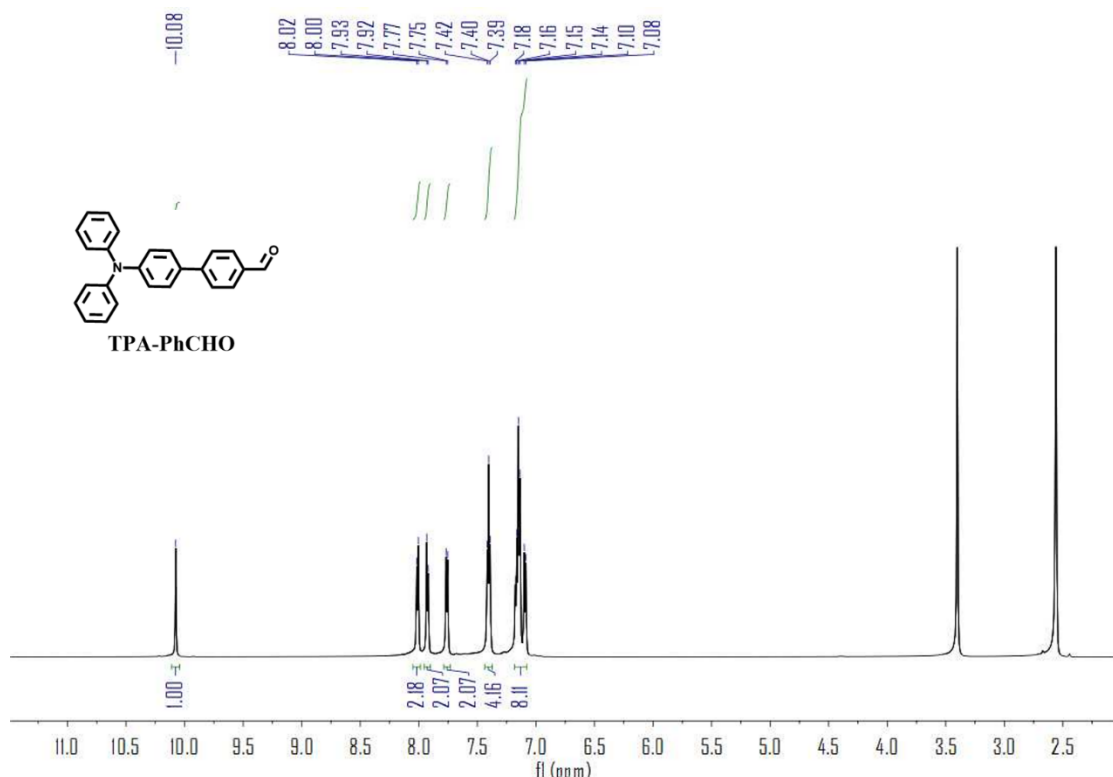


Figure S2 ¹H NMR spectrum of TPA-PhCHO in *d*6-DMSO.

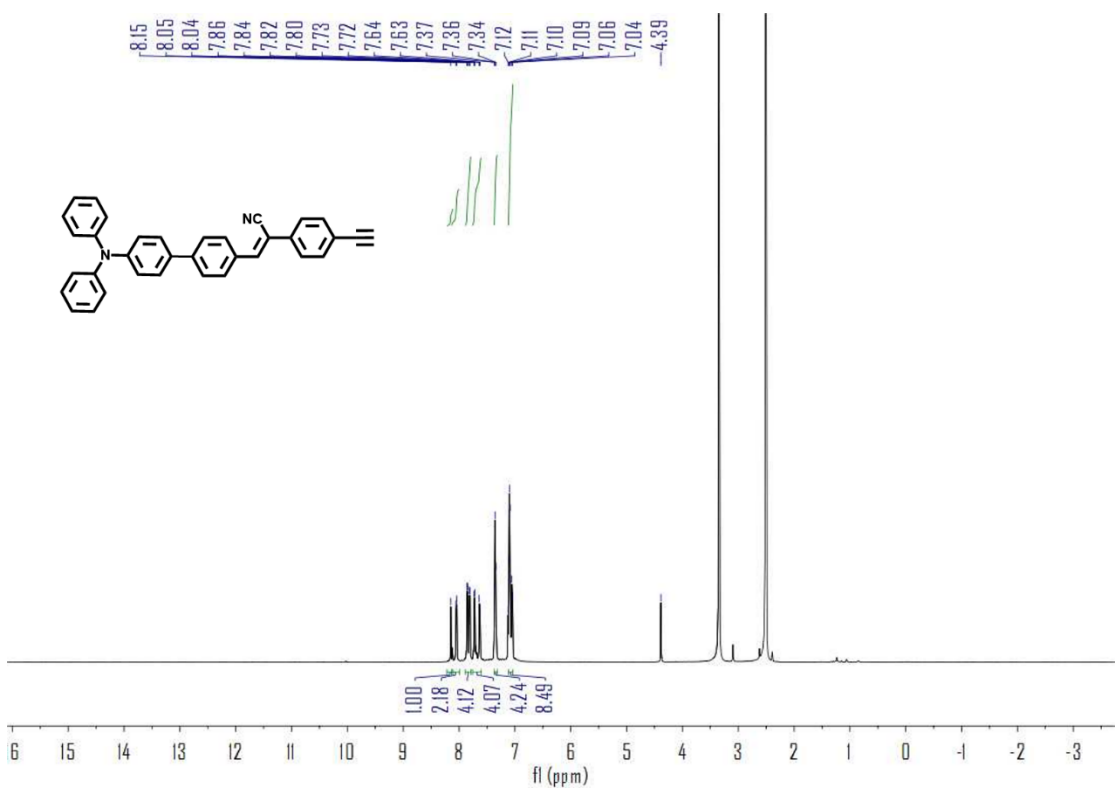


Figure S3 ^1H NMR spectrum of PS-1 in d_6 -DMSO.

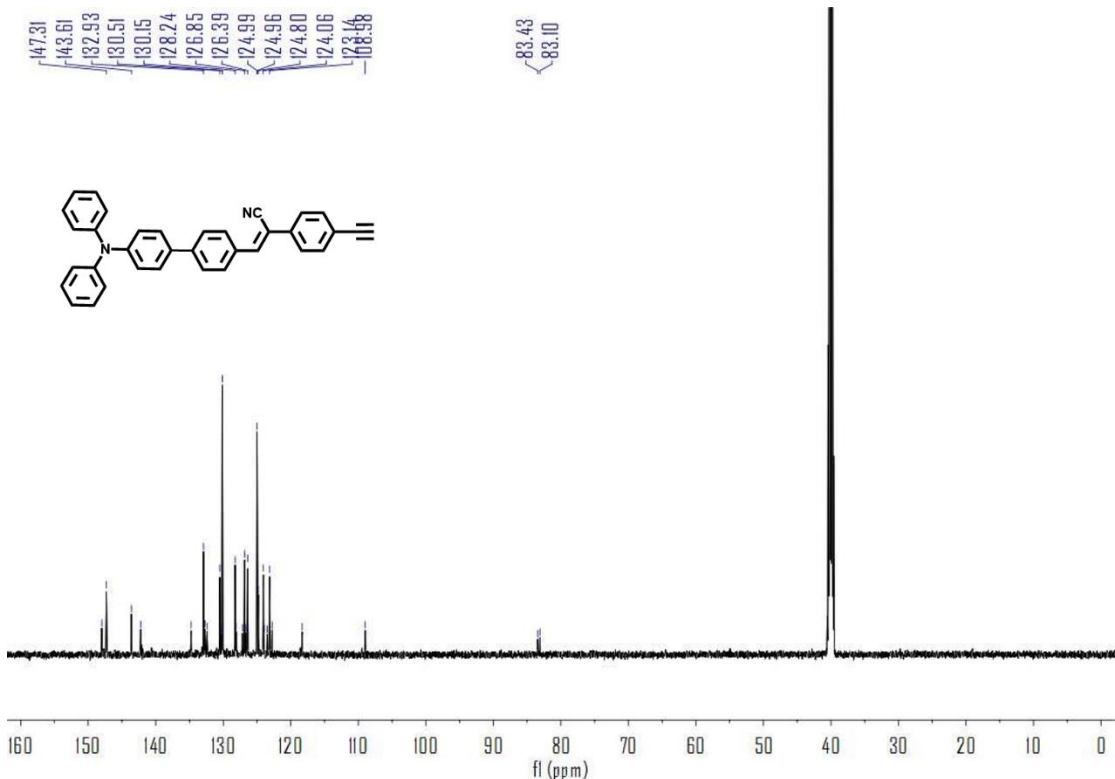
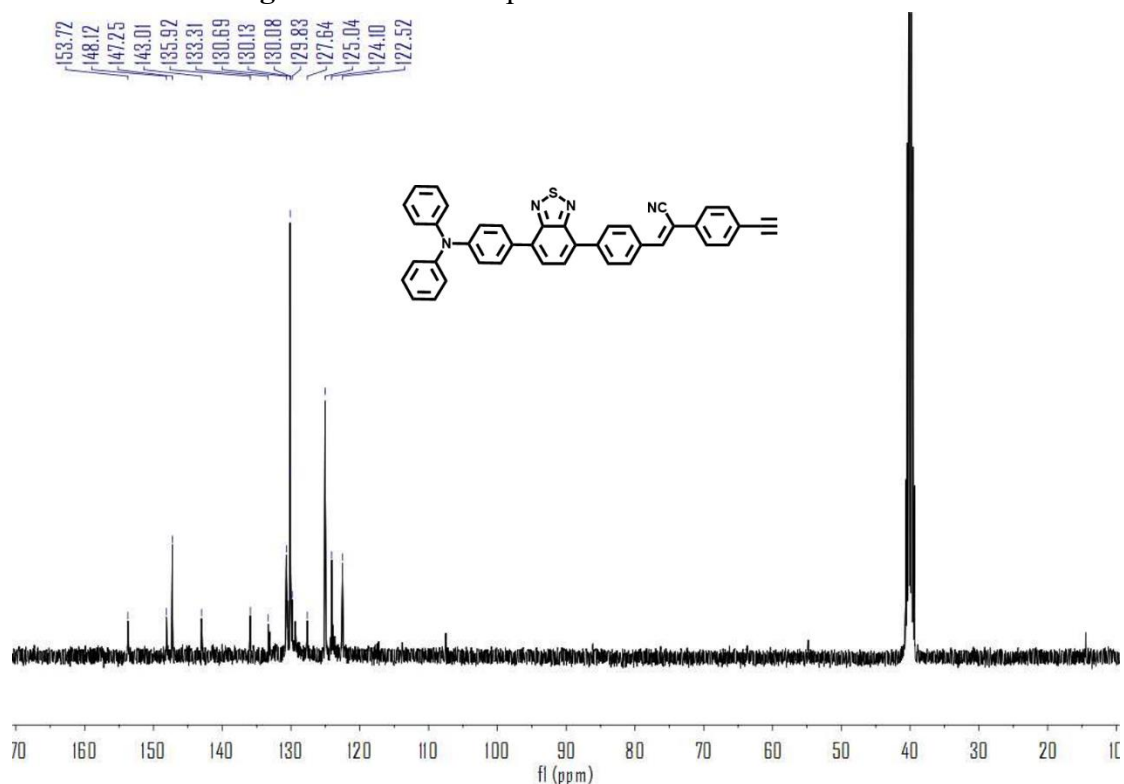
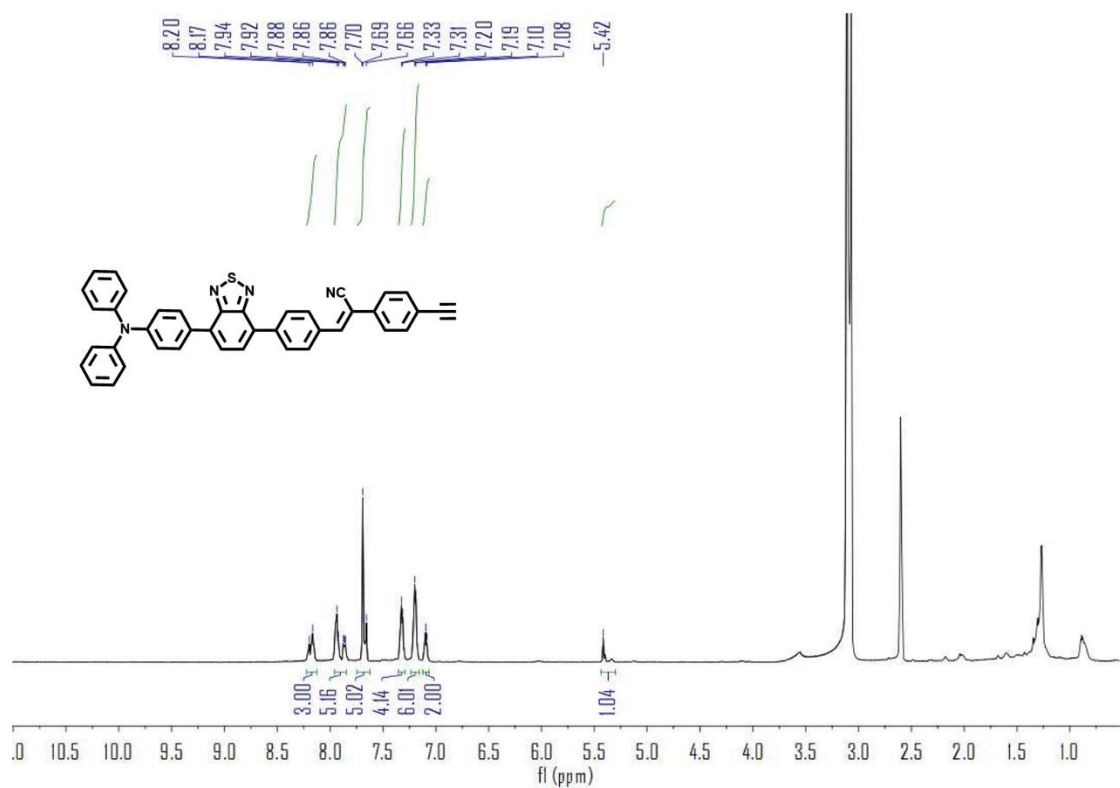


Figure S4 ^{13}C NMR spectrum of PS-1 in d_6 -DMSO.



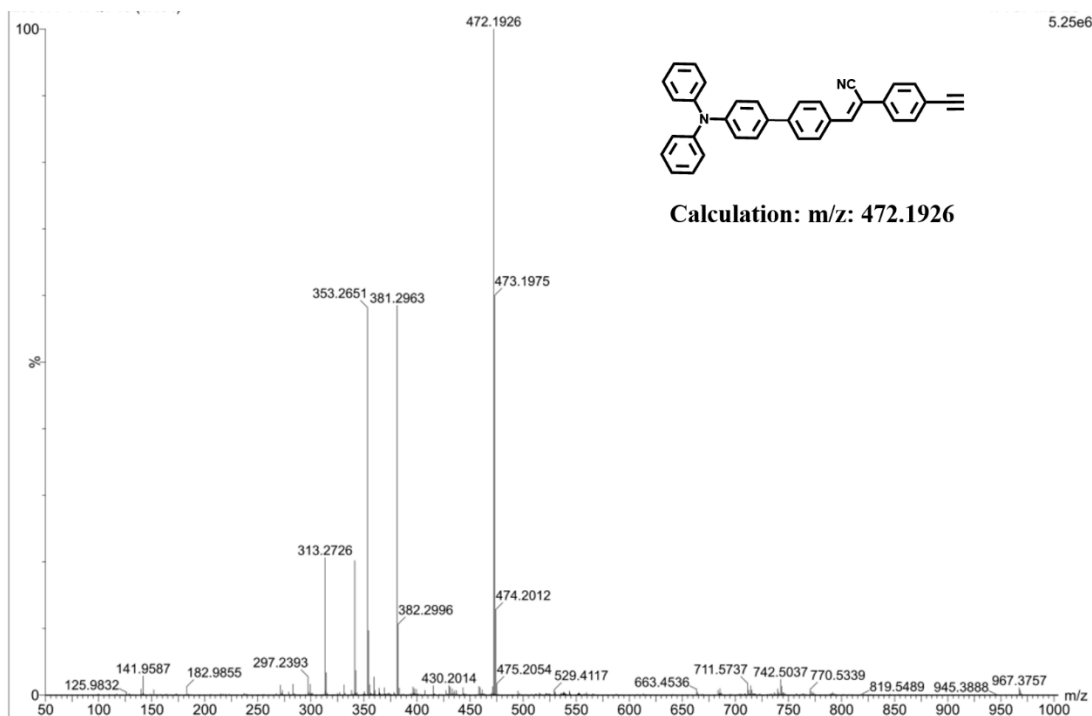


Figure S7 High resolution mass spectrum (HRMS) of spectrum of PS-1.

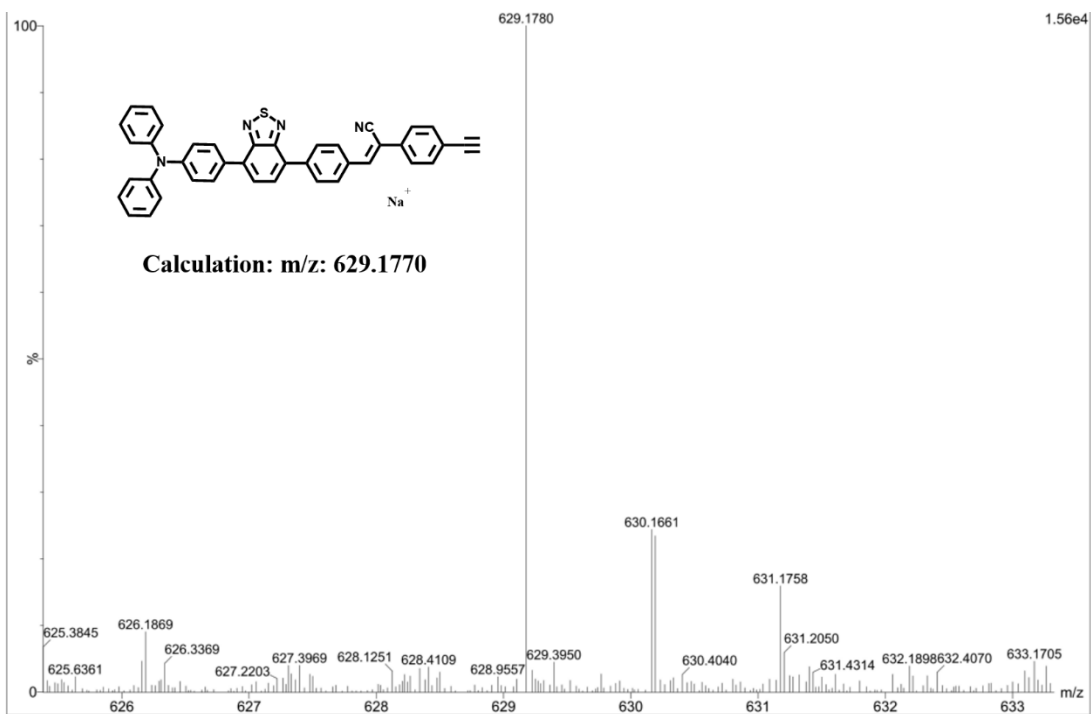


Figure S8 High resolution mass spectrum (HRMS) of spectrum of PS-2.

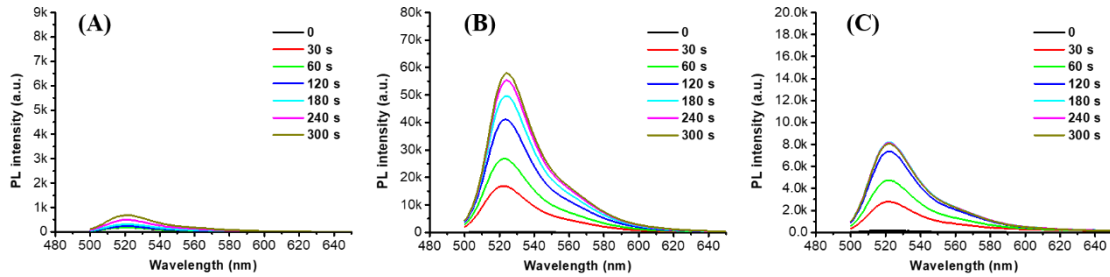


Figure S9 PL spectra of (A) pure DCFH, (B) DCFH mixed PS-1, (C) DCFH mixed PS-2 upon white light irradiation for different time point, PS-1 (5 μ M), PS-2 (5 μ M), DCFH (10 μ M), white light power: 30 mW/cm 2 .

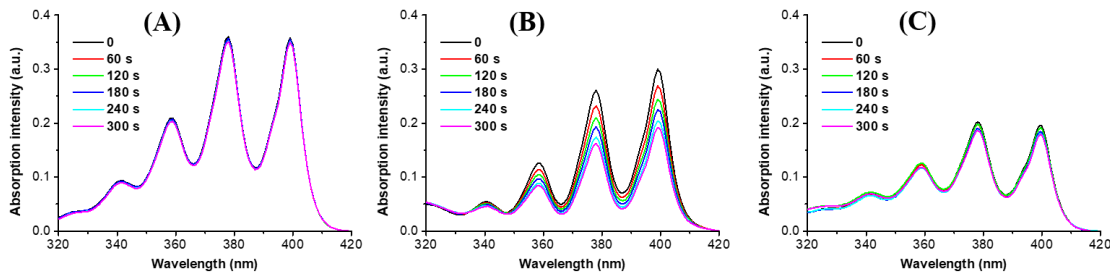


Figure S10 Absorption spectra of (A) pure ABDA, (B) ABDA mixed PS-1, (C) ABDA mixed PS-2 upon white light irradiation for different time point, PS-1 (5 μ M), PS-2 (5 μ M), ABDA (20 μ M), white light power: 30 mW/cm 2 .

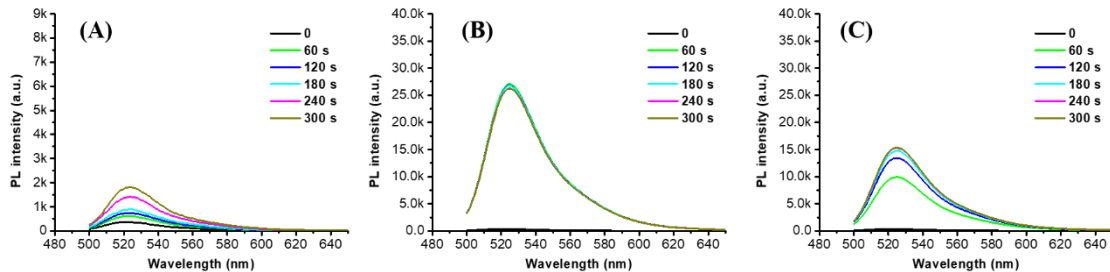


Figure S11 PL spectra of (A) pure DHR123, (B) DHR123 mixed PS-1, (C) DHR123 mixed PS-2 upon white light irradiation for different time point, PS-1 (2 μ M), PS-2 (2 μ M), DHR123 (10 μ M), white light power: 30 mW/cm 2 .

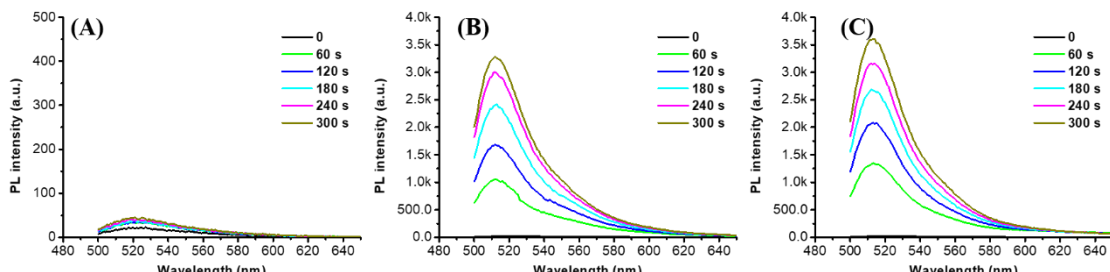


Figure S12 PL spectra of (A) pure HPF, (B) HPF mixed PS-1, (C) HPF mixed PS-2 upon white light irradiation for different time point, PS-1 (2 μ M), PS-2 (2 μ M), HPF (10 μ M), white light power: 30 mW/cm 2 .

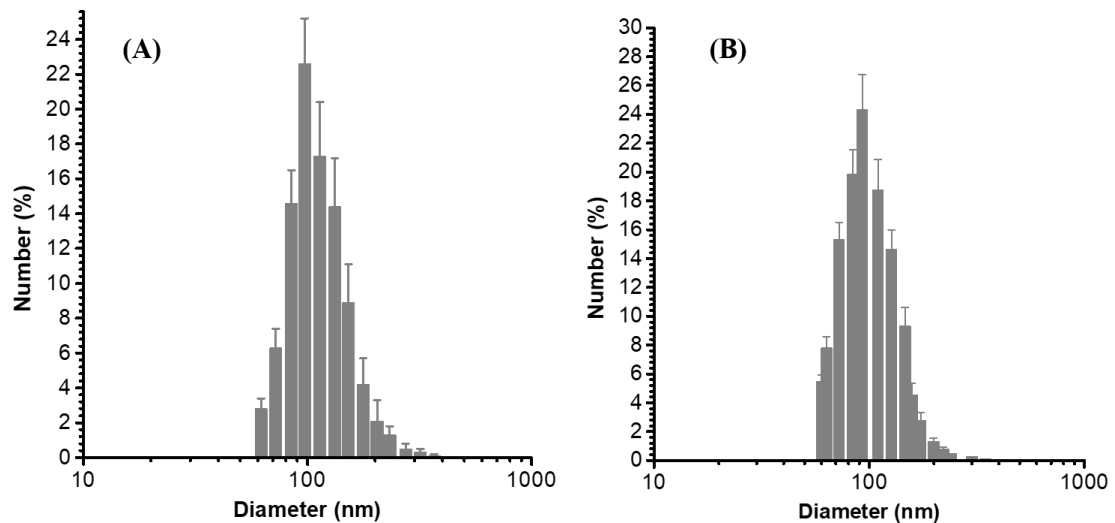


Figure S13 (A) DLS measurement of PS-1@BSA NPs, (B) DLS measurement of PS-2@BSA NPs.

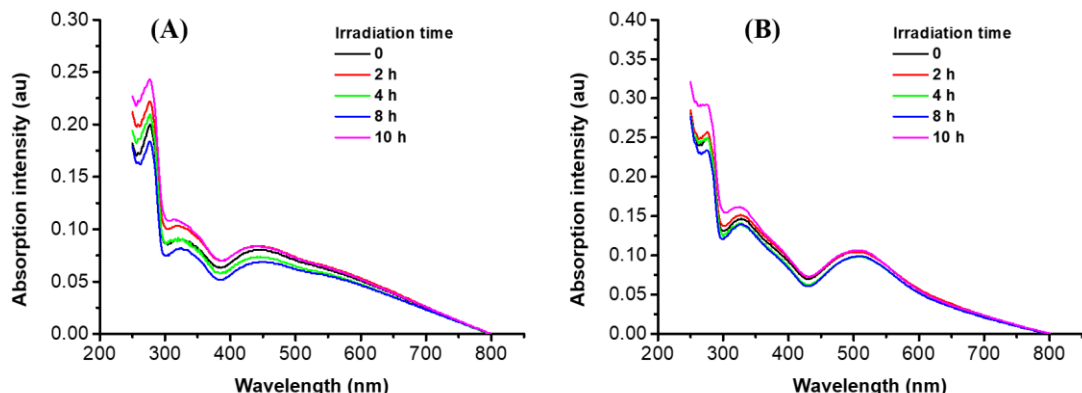


Figure S14 (A) UV absorption spectra of PS-1@BSA NPs and PS-2@BSA NPs. Concentration of PS-1@BSA NPs and PS-2@BSA NPs is 30 $\mu\text{g}/\text{mL}$.

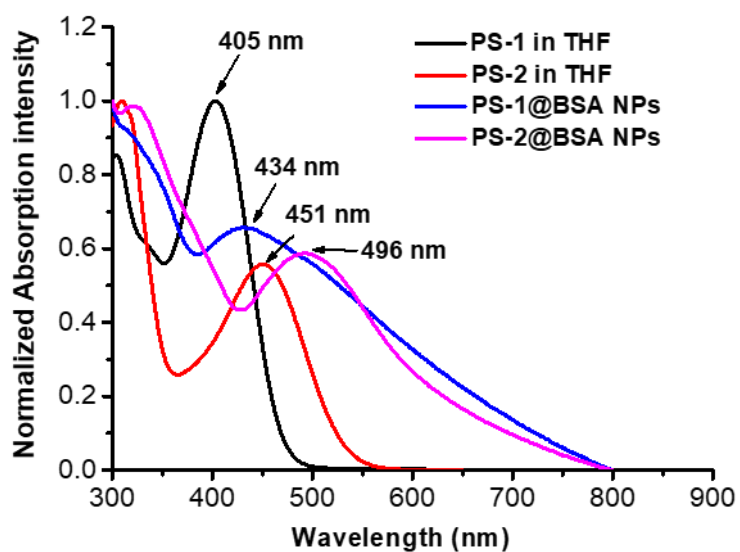


Figure S15 UV-Vis absorption spectra of PS-1/PS-2/PS-1@BSA NPs and PS-2@BSA

NPs, [PS-1] = 10 μ M, [PS-2] = 10 μ M, [PS-1@BSA NPs] = 50 μ g/mL, [PS-2@BSA NPs] = 50 μ g/mL.

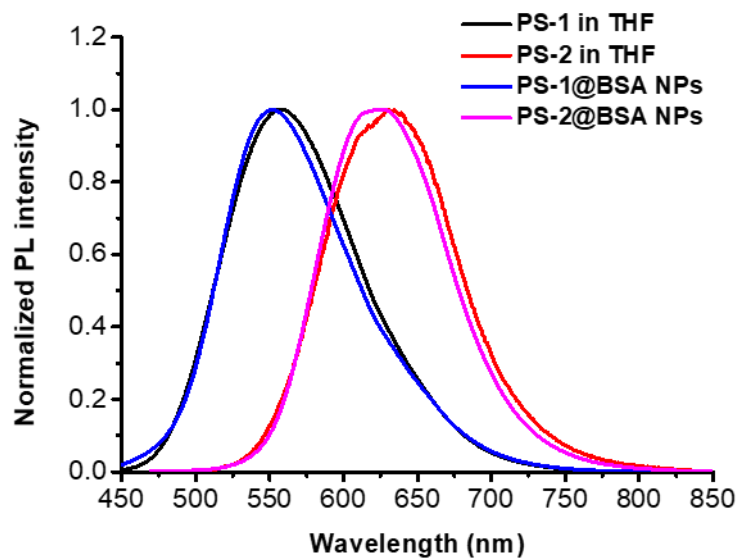


Figure S16 PL spectra of PS-1/PS-2/PS-1@BSA NPs and PS-2@BSA NPs, [PS-1] = 10 μ M, [PS-2] = 10 μ M, [PS-1@BSA NPs] = 50 μ g/mL, [PS-2@BSA NPs] = 50 μ g/mL.

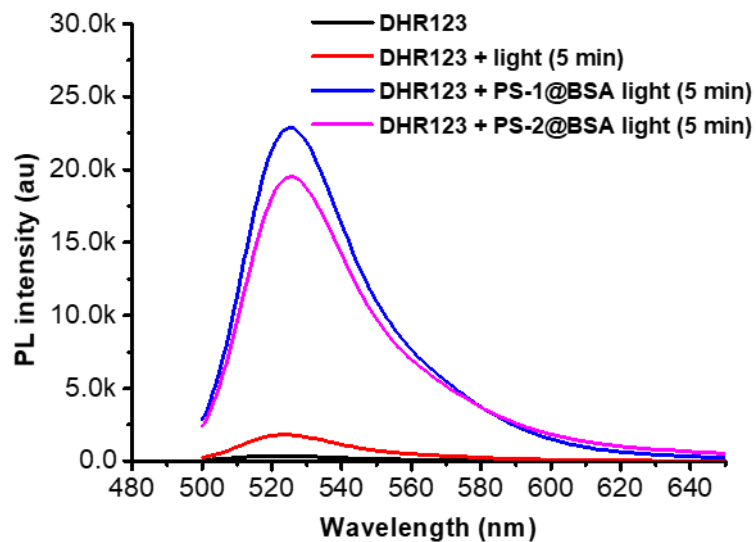


Figure S17 PL spectra of pure DHR123, DHR123 mixed PS-1@BSA NPs or PS-2@BSA NPs, [PS-1@BSA NPs] = 10 μ g/mL, [PS-2@BSA NPs] = 10 μ g/mL, [DHR123] = 10 μ M, white light power: 30 mW/cm².

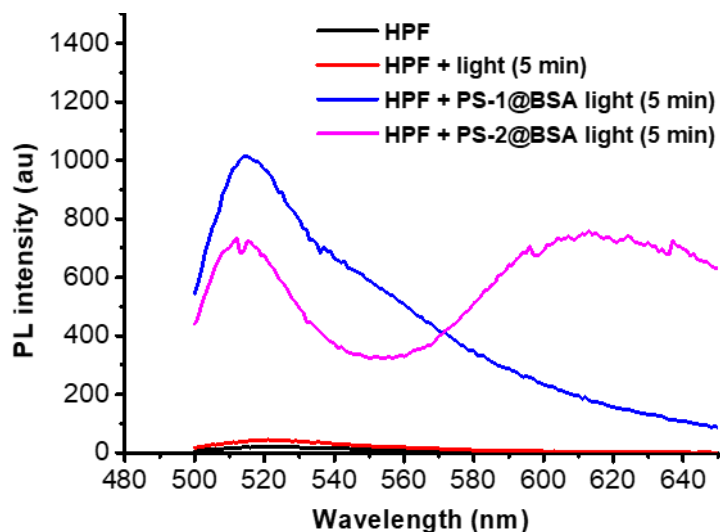


Figure S18 PL spectra of pure HPF, HPF mixed PS-1@BSA NPs or PS-2@BSA NPs, [PS-1@BSA NPs] = 10 $\mu\text{g}/\text{mL}$, [PS-2@BSA NPs] = 10 $\mu\text{g}/\text{mL}$, [HPF] = 2 μM , white light power: 30 mW/cm^2 .

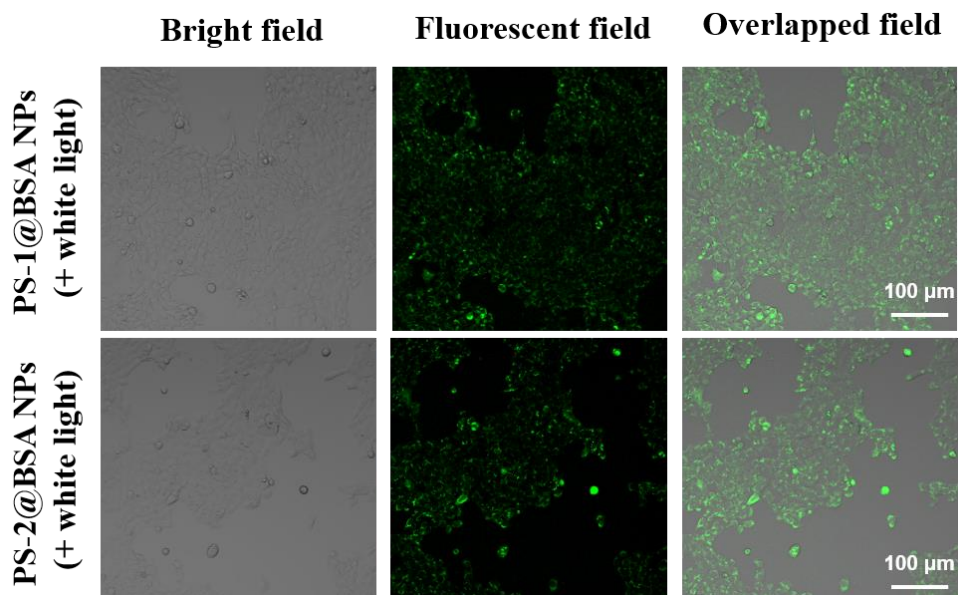


Figure S19 CLSM images of B16-F10 cancer cells mixed DCFH probe and PS-1@BSA NPs and PS-2@BSA NPs after white light irradiation of 5 min. Scale bar = 100 μm . [DCFH] = 10 μM , [PS-1@BSA NPs] = 100 $\mu\text{g}/\text{mL}$, [PS-2@BSA NPs] = 100 $\mu\text{g}/\text{mL}$, white light: 30 $\text{mW}\text{ cm}^{-2}$.

References:

- (1) Xu, Y.; Xie, Y.; Wan, Q.; Tian, J.; Liang, J.; Zhou, J.; Song, M.; Zhou, X.; Teng, M. Mechanism research of type I reactive oxygen species conversion based on molecular and aggregate levels for tumor photodynamic therapy. *Aggregate* **2024**, *5*, e612.

Declaration of interests

The authors declare that they have no known competing financial interests or personal relationships that could have appeared to influence the work reported in this paper.

The authors declare the following financial interests/personal relationships which may be considered as potential competing interests:

Light-Triggered Click Reaction to Fabricate Bright Bovine Serum Albumin Encapsulates Photosensitizer's Nanoparticles for Effective Photodynamic Therapy of Melanoma Cells

Yifan Li¹, Yitao Fan¹, Qian Liu², Xuya Wang², Yuxia Jin², Muzhou Teng*^{1,2}

1. Department of Dermatology, The Second Hospital & Clinical Medical School, Lanzhou University, Lanzhou, China.

2. Gansu Provincial Maternity and Child-Care Hospital (Gansu Provincial Central Hospital), Lanzhou, China.

Corresponding author: Prof. Muzhou Teng (smutmz@126.com)

Abstract

Photodynamic therapy (PDT) has emerged as a promising anticancer strategy due to its non-invasive nature and precise spatiotemporal control. However, conventional photosensitizers (PSs) suffer from aggregation-caused quenching (ACQ), poor hydrophilicity, and serious oxygen dependence, limiting their clinical utility. To address these challenges, we developed an efficient strategy to fabricate hydrophilic aggregation-induced emission (AIE)-active Bovine Serum Albumin (BSA) Encapsulates PSs via an effective light-mediated thiol-yne click reaction. By designing alkynyl-functionalized AIE-active PSs with strong

generating capability of type I/II reactive oxygen species (ROS), we achieved fast combination with thiol-rich BSA under UV light irradiation, forming stable BSA@AIE-active PSs' nanoparticles (NPs). The resulting NPs exhibited excellent water dispersibility, bright fluorescence and intense ROS generation. *In vitro* studies demonstrated their outstanding PDT effect to melanoma cell (B16-F10) under white light irradiation. This work proposed a universal, scalable, and eco-friendly platform for constructing AIE-active hydrophilic PS's NPs, overcoming longstanding hurdles in PS's hydrophobicity and fabrication complexity.

Keywords: Aggregation-induced emission, click reaction, photodynamic therapy, bovine serum albumin, melanoma cell

Introduction

Photodynamic therapy (PDT), as a non-invasive and spatiotemporally controllable treatment technology, has attracted increasing research interests in biomedical field.^[1-3] By leveraging light-activated photosensitizers (PSs) to generate cytotoxic reactive oxygen species (ROS), PDT offers an effective approach to eliminate cancer cells while minimizing damage to healthy tissues.^[4] However, some disadvantages of conventional PSs make them difficult to achieve highly efficient practical applications, such as typical and head-scratching aggregation-caused quenching (ACQ) effect,^[5] poor water solubility, and serious oxygen

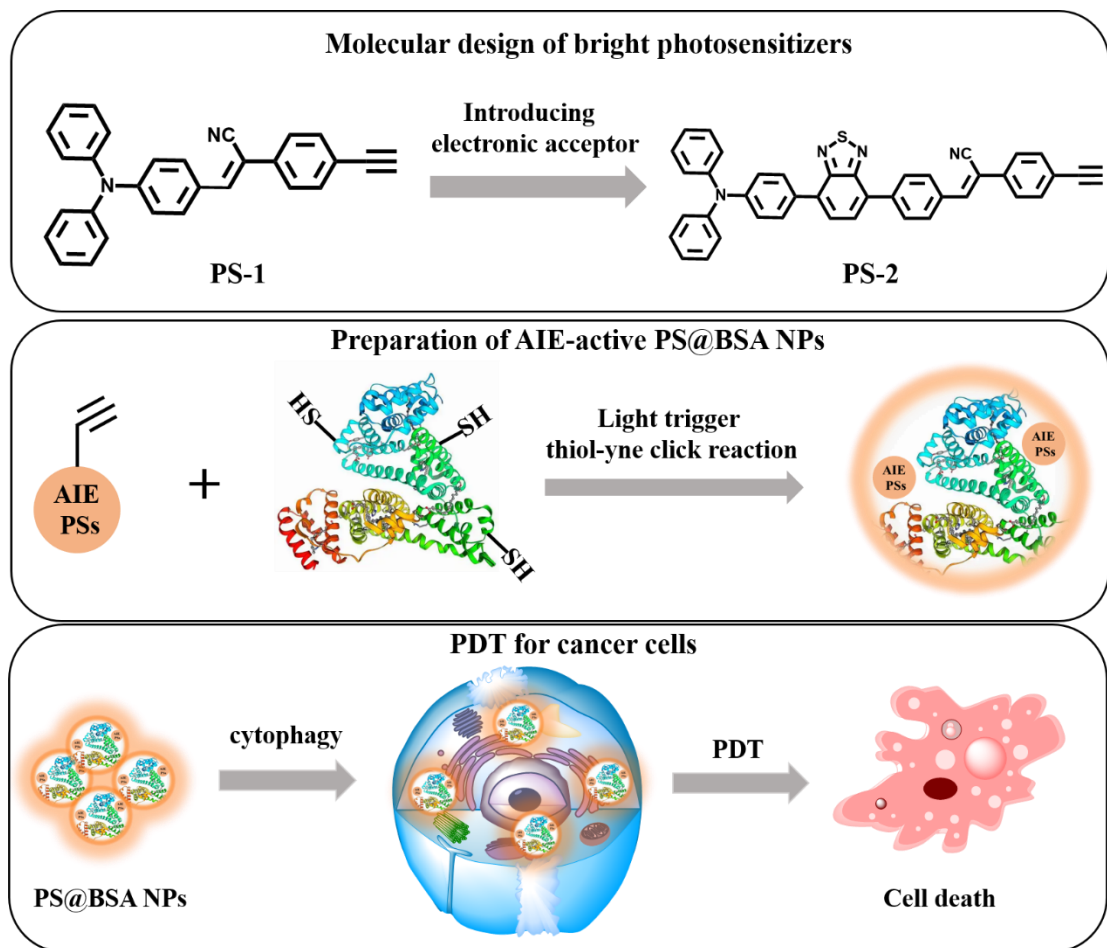
dependence.^[6] These drawbacks often lead to reduced fluorescence and ROS generation efficiency, suboptimal biocompatibility, and limited therapeutic efficiency. In recent years, aggregation-induced emission (AIE)-active PSs have emerged as a revolutionary class of photosensitizers (PSs),^[7-8] addressing effectively the ACQ problem by exhibiting enhanced luminescence and ROS generation in the aggregated state.^[9-11] Despite their a series of advantages, the hydrophobic nature of most aromatic AIE-active PSs poses challenges in achieving stable aqueous dispersion, necessitating additional chemical modifications or carrier systems to improve biocompatibility.^[12-15] This trade-off between functionality and practicality underscores the urgent need for innovative strategies to streamline the fabrication of AIE-based nanoplatforms without compromising performance.

Click chemistry, renowned for its high efficiency, selectivity, and mild reaction conditions, has become an important protocol to fabricate biomedical materials and modify surface,^[16-19] which has promising applications in the fields of bioconjugation and nanomaterial engineering. Among its diverse reactions, the light-triggered thiol-yne click reaction stands out for its spatiotemporal control and catalyst-free nature, making it particularly suitable for biomedical applications.^[20-23] By exploiting the rapid and specific coupling between alkyne and thiol groups under light irradiation, this strategy enables precise functionalization of biomolecules

while preserving their native activity. Building on this principle, we herein report a novel methodology for constructing hydrophilic AIE-active PSs' nanoparticles via a one-step photo-click reaction between alkynyl-functionalized AIE-active PSs and thiol group contained Bovine Serum Albumin (BSA). This approach not only circumvents the need for toxic catalysts but also integrates the advantages (aggregation enhances fluorescence and ROS efficiency) of AIE-active PSs with the inherent biocompatibility of BSA, yielding nanoscale PSs with superior water dispersibility, better biocompatibility and effective PDT to cancer cells.

Based on above description, in this research work, two type BSA encapsulated AIE-active PSs' nanoparticles (NPs) were designed and prepared. First, the incorporation of alkyne group into AIEgens to fabricate two donor (D)-acceptor (A) type PSs (namely as PS-1 and PS-2) by ingenious chemical synthesis. Then, BSA was used to react with above AIE-active PSs to afford AIE-active PSs' NPs via light-mediated thiol-yne click addition reaction (**Scheme 1**). The detail synthetic processes were described in the supporting information (**Figure S1**). For the molecular design, PS-2 had additional electronic acceptor of benzothiadiazole than PS-1, which was expected to achieve red fluorescence of BSA@PS NPs. Experimental result showed that resulting nanocomposites retain the AIE-active PSs' robust ROS generation capability. Systematic evaluations demonstrated that these BSA-based AIE-active PSs' NPs form small

nanoparticles with diameters of near 100 nm. *In vitro* studies further revealed their potent anticancer cells efficacy under light irradiation, achieving over 90% cancer cell ablation, alongside excellent photostability and minimal dark toxicity. This work represents an effective method in fabricating biocompatible AIE-active PS's NPs, which is expected to provide a foundational framework for the industrial-scale production of biocompatible AIE-active PSs.



Scheme 1 Demonstration of molecular structures of PSs and light trigger thiol-yne click reaction to fabricate AIE-active PS@BSA nanoparticles for photodynamic anticancer cells.

Results and discussion

Synthesis and characterization of PS-1 and PS-2

Targeted PS-1 and PS-2 were synthesized by combining typical chemical reaction of Suzuki reaction and Knoevenagel condensation reaction, which was purified by the filtration and wash for three times by using heated ethanol with a better yields of 83% and 72%. Firstly, molecular structure of PS-1 was constructed by adopting triphenylamine (TPA) as electronic donor and phenylacetonitrile as electronic acceptor. Differently, PS-2 had additional electronic acceptor of benzothiadiazole than PS-1, which was expected to redshift maximal fluorescence peak.^[24] Chemical structures of intermediate and final products were clearly characterized by hydrogen/carbon nuclear magnetic resonance ($^1\text{H}/^{13}\text{C}$ NMR) and high-resolution mass spectra (**Figure S2-8**).

Photophysical properties and theoretical calculation

The photophysical properties of PS-1 and PS-2 were initially evaluated (**Figure 1A**). Both compounds demonstrated good solubility in tetrahydrofuran (THF), with absorption maxima observed at 405 nm and 495 nm, respectively. Their photoluminescence (PL) spectra with maximal emissive wavelength peaked at 557 nm and 629 nm, respectively. Therefore, photophysical property of absorption and fluorescent spectra suggested that PS-1 emitted yellow fluorescence and PS-2 emitted red fluorescence, ascribed to the enhanced intramolecular charge transfer (ICT) effect after inserting electronic acceptor of benzothiadiazole in the PS-2.^[25-26] Notably, PS-1 achieved a significantly higher photoluminescence

quantum yield (32.7%) in neat film compared to PS-2 (11.4%), it might be contributed to the intramolecular charge transfer (ICT) effect quenched fluorescence.^[27] In addition to this reason, different molecular packing modes of these two emitters might cause the difference on their photoluminescence quantum yields.^[28-29] Theoretical analyses of frontier molecular orbital distributions revealed electron transition process (**Figure 1B**). For the highest occupied molecular orbital (HOMO) of PS-1, electron density localized predominantly on the triphenylamine unit, while the electron of the lowest unoccupied molecular orbital (LUMO) concentrated at phenylacetonitrile unit. Differently, electrons of HOMO of PS-2 distributed on the units of triphenylamine and benzothiadiazole, while the LUMO's electrons also concentrated at benzothiadiazole and phenylacetonitrile unit. Theoretical calculation of transition decay was carried out, PS-1 and PS-2 had the transition decay of 4.63 Debye and 5.71 Debye, the larger transition decay of PS-2 was well match with its longer absorption and emissive wavelength.

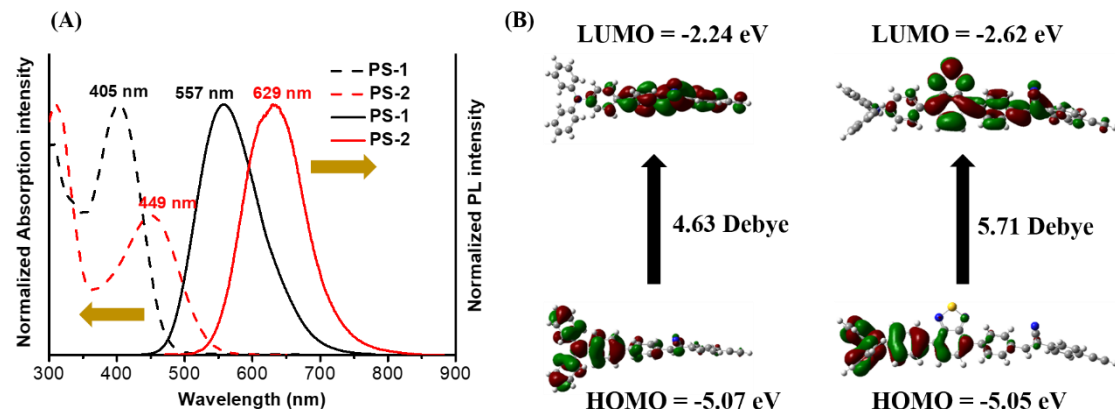


Figure 1 (A) UV-vis absorption and PL spectra of PS-1 and PS-2 in THF solvent; (B)

Electron distribution of HOMOs/LUMOs and their calculated values based on b3lyp/6-31g(d,p). [PS-1] = 10 μ M, [PS-2] = 10 μ M.

To explore the correlation between solvent polarity and emitter's fluorescence, ultraviolet visible (UV-vis) absorption and photoluminescence spectra of the two emitters were recorded in different organic solvents with different polarity. Absorption spectra showed small maximal spectral shift accompanying with increased solvent polarity (**Figure 2A-B**), indicating negligible solvatochromic effect of ground-state electronic structure to environmental polarity. Oppositely, excited-state property displayed obvious polarity-dependent trend, evidenced by progressive emission redshift and fluorescence attenuation across the solvent gradient (**Figure 2C-D**). PS-1 exhibited a bathochromic displacement from 493 nm in hexane to 634 nm in dimethyl sulfoxide (DMSO), while PS-2 manifested analogous solvatochromic behavior, shifting from 538 nm to 674 nm under same condition (**Figure 2E-F**). This pronounced excited-state sensitivity stemmed from polar media-induced stabilization of ICT state, as supported by spectral progression trend.^[30] The solvent-dependent spectral alterations conclusively validate strong ICT attributes in both emitters, with solvation effects preferentially stabilizing charge-separated excited-state configurations in highly polar environments.

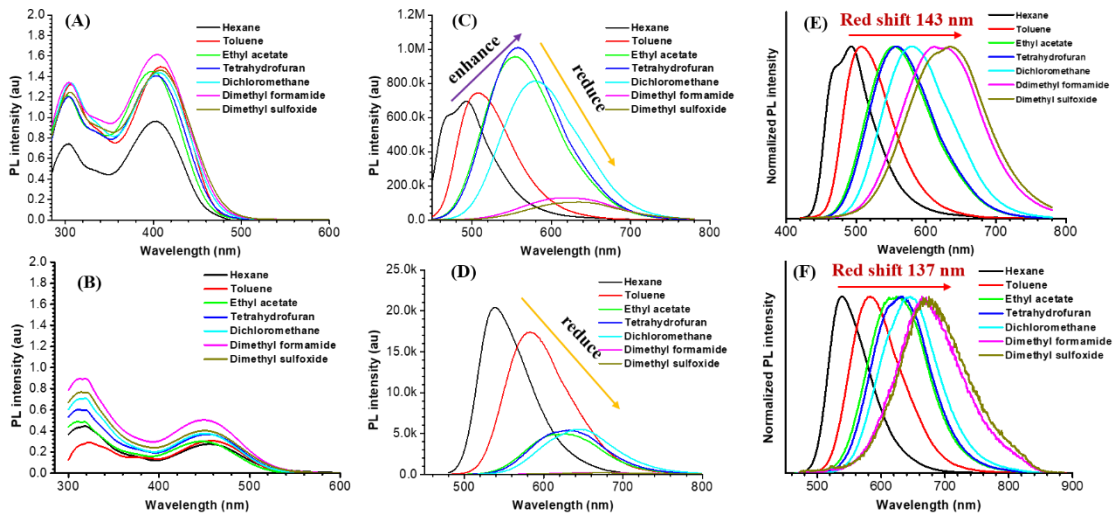


Figure 2 Absorption spectra of PS-1 (A) and PS-2 (B) in different organic solvents; PL spectra of PS-1 (C) and PS-2 (D) in different organic solvents; Normalized PL spectra of PS-1 (E) and PS-2 (F) in different organic solvents. Concentration: 20 μ M.

AIE property of both emitters were systematically evaluated. Firstly, the PLQYs of these two emitters in DMSO and neat film were measured. the PLQYs of PS-1 and PS-2 were detected as 22.5% and 18.9% in DMSO. In neat film, the PLQYs of PS-1 and PS-2 were 32.7% and 11.4%, above results suggested preliminarily that PS-1 had aggregation enhanced emission (AEE) nature, but PS-2 might show aggregation caused fluorescence quench effect. To further confirm their AIE property, as depicted in **Figure 3A-B**, their PL spectra displayed distinct emission trends in DMSO/H₂O mixture with incremental aqueous content. In pure DMSO, the emitters exhibited orange fluorescence, contrasting sharply with classical AIE luminogens (AIEgens) like tetraphenylethylene (TPE) and hexaphenylsilole (HPS),^[31-32] where dissolved in good solvents typically exhibited very weak fluorescence. For the PS-1, when increasing the water fraction to 60%, fluorescence intensity enhanced progressively

alongside a 76 nm blue shift in maximal emission peak. The improved fluorescent intensity was contributed to the AIE effect, while blue shift of maximal emissive peak within 60% water fraction could be attributed to the changed polar environment from high-polarity DMSO solvent to low-polarity aggregates. Similarly, PS-2 also showed that the fluorescence intensity decreased first and then increased, which was contributed to the synergistic effect of “AIE+TICT”.^[33]

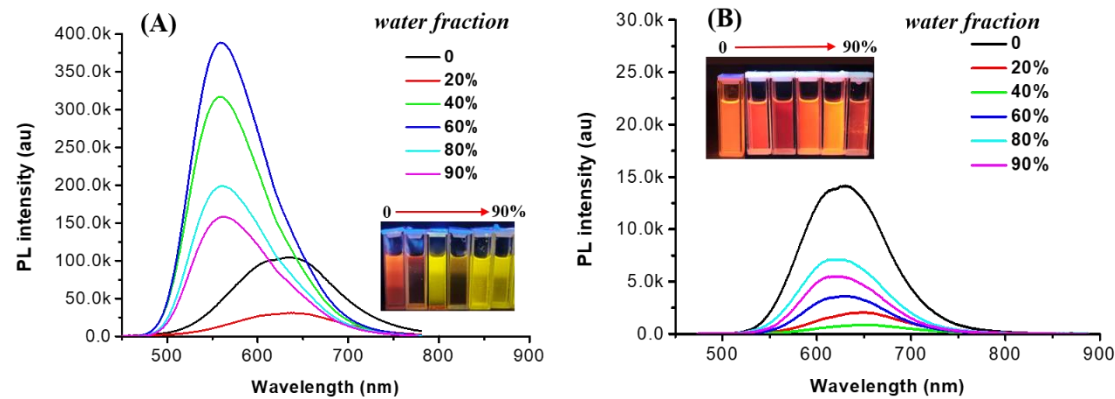


Figure 3 Fluorescent spectra of PS-1 (A) and PS-2 (B) in DMSO/H₂O mixture solvents with different water fraction. Concentration: 20 μM.

Detection of reactive oxygen species

PDT functions as a non-invasive therapeutic approach that leverages light-activated PSs to generate cytotoxic ROS. This mechanism relies on biocompatible PSs absorbing visible light to generate triplet excited states, which then facilitates energy and electron transfer to molecular oxygen. To quantitatively assess ROS production in PS-1 and PS-2, we utilized DCFH dye, a fluorescent probe emitting at maximal 524 nm upon oxidation by ROS. Both PSs demonstrated efficient ROS generation under white light irradiation, consistent with their strong visible-light absorption capability.

Control experiments (**Figure S9A**) revealed minimal background fluorescence from 2',7'-dichlorofluorescein diethylenetriacetate (DCFH-DA) alone under illumination. In contrast, solutions containing PS-1 and PS-2 exhibited substantial fluorescence enhancement upon light exposure (**Figure 4A** and **Figure S9B-C**). Comparative analysis of fluorescent intensity amplification conclusively identified PS-1 as the superior ROS generator under same irradiation condition, achieving markedly higher efficiency than PS-2.

Photodynamic activity generally proceeds through two distinct routes for ROS production: (1) energy transfer from the triplet-excited state of PSs to molecular oxygen, producing singlet oxygen (${}^1\text{O}_2$), (2) electron transfer reactions that generate superoxide radicals (O_2^-) and hydroxyl radicals ($\cdot\text{OH}$).^[34] To determine the predominant ROS species generated by PS-1 and PS-2, we utilized the selective ${}^1\text{O}_2$ probe of 9,10-anthracenediyl-bis(methylene)-dimalonic acid (ABDA). The anthracene-based compound ABDA specifically reacts with ${}^1\text{O}_2$ through irreversible endoperoxide formation, enabling quantification via absorbance loss at characteristic wavelengths. Initial control measurement showed negligible absorbance changes in only ABDA solution under prolonged white-light illumination (**Figure 4B** and **Figure S10**). However, systems incorporating PS-1 or PS-2 exhibited marked absorbance reduction, confirming effective ${}^1\text{O}_2$ generation by both PSs. Comparative analysis revealed PS-1 induced

significantly greater ABDA degradation than PS-2, establishing its superior ${}^1\text{O}_2$ production capability under equivalent irradiation conditions.

The generation of type I ROS, specifically O_2^- and $\cdot\text{OH}$, was systematically investigated using fluorescent probes of dihydrorhodamine 123 (DHR123) and hydroxyphenyl fluorescein (HPF).^[35] Initial verification of O_2^- production was conducted through DHR123, a non-fluorescent compound that exhibits distinct green fluorescence emission at 525 nm upon interaction with O_2^- . As demonstrated in **Figure 4C** and **Figure S11**, control experiment revealed minimal fluorescence variation in pure DHR123 solutions under 5-minute irradiation. However, significant fluorescence enhancement was observed when PS-1 or PS-2 solution containing DHR123 were exposed to white light, confirming effective O_2^- generation. Subsequent $\cdot\text{OH}$ detection using hydroxyphenyl fluorescein (HPF) probe showed differential radical production between compounds. **Figure 4D** and **Figure S12** illustrated that the PS-2 and HPF combination exhibited stronger fluorescence intensity compared to PS-2 and HPF combination, indicating superior $\cdot\text{OH}$ generation efficiency in PS-2. Therefore, according to above analysis, PS-1 has better O_2^- and ${}^1\text{O}_2$ generation, while PS-2 shows more efficient $\cdot\text{OH}$ generation than PS-1.

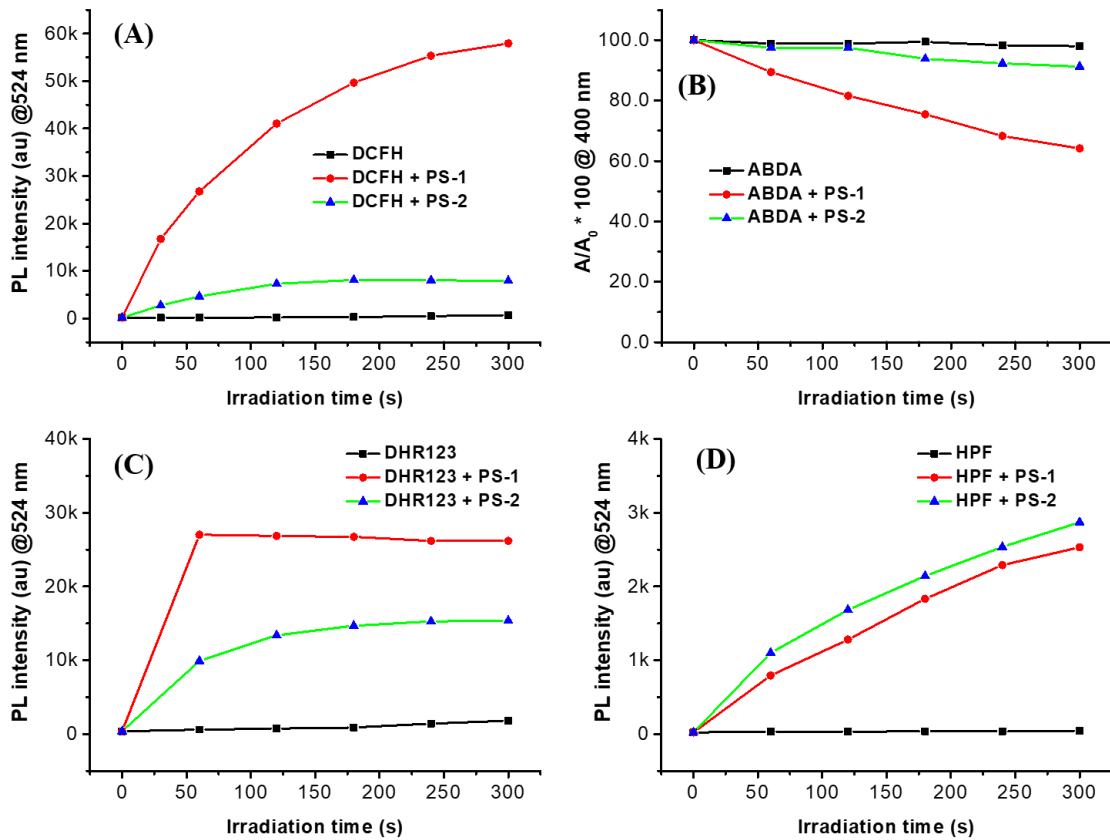


Figure 4. (A) Measurement of total ROS of PS-1 (5 μ M) and PS-2 (5 μ M) by using DCFH (10 μ M) probe upon white light irradiation, (B) access of $^1\text{O}_2$ generation with the decomposition of ABDA (20 μ M) probe after mixing PS-1 (5 μ M) and PS-2 (5 μ M) upon white light irradiation, (C) access of O_2^- generation of PS-1 (2 μ M) and PS-2 (2 μ M) by using DHR123 (10 μ M) probe upon white light irradiation, (D) access of $\cdot\text{OH}$ generation of PS-1 (2 μ M) and PS-2 (2 μ M) by using HPF (10 μ M) probe upon white light irradiation, white light power: 30 mW/cm².

PDT effect of B16-F10 cancer cells

Due to the favorable ROS generation and fluorescence efficiency of PS-1 and PS-2, their PDT potential was assessed at the cellular level by choosing B16-F10 cancer cells as research object. However, both PSs exhibited pronounced hydrophobicity, hindering cellular uptake. To address this limitation, the natural polymer of BSA was employed to link covalently with PSs to enhance their hydrophilicity because alkynyl of PSs could happen click reaction with thiol group of BSA, therefore yielding stable PS-

1@BSA NPs and PS-2@BSA NPs with enhanced aqueous dispersibility. Dynamic light scattering (**Figure S13A-B**) revealed hydrodynamic diameters of near 100 nm for PS-1@BSA NPs and PS-2@BSA NPs, with nanoscale dimensions promoting efficient cellular uptake. Their zeta potentials were measured as -36.43 mV and -37.03 mV, and the encapsulation efficiency of PS-1@BSA NPs and PS-2@BSA NPs are about 25.0% and 34.7%. Furthermore, two NPs have better photostability after frequent irradiation by UV light because of not obvious reduction of absorption intensity (**Figure S14**). Next, photophysical properties and ROS performance of PS-1@BSA NPs and PS-2@BSA NPs were characterized. As shown in **Figure S15**, comparing the absorption spectra of PS-1/ PS-1@BSA NPs and PS-2/ PS-2@BSA NPs, it can be known that absorption spectra of BSA-based NPs show a significant redshift phenomenon. For example, PS-1 in THF had the maximal absorption spectrum of 405 nm, but red-shifted to the 434 nm after forming PS-1@BSA NPs. PS-2@BSA NPs showed maximal absorption wavelength of 496 nm, which was larger than PS-2 in THF with maximal absorption peak of 451 nm. Oppositely, comparing with PS-1/PS-2 in THF, the maximal emissive peaks of PS-1@BSA NPs and PS-2@BSA NPs showed a slight blueshift (**Figure S16**). Probes of DHR123 and HPF were used to characterize the type I ROS generation of PS-based BSA NPs, as shown in **Figure S17-18**, fluorescent intensity from DHR123 and HPF showed obvious enhancement,

suggesting an effective generation of O_2^- and $\cdot OH$.

To evaluate intracellular ROS production, the DCFH fluorescent probe was utilized, B16-F10 cancer cells co-treated with PS@BSA NPs exhibited bright green fluorescence, confirming effective ROS generation (**Figure S19**). According to **Figure 5C-D**, cytocompatibility study demonstrated that over 95% cell viability at high PS@BSA NPs concentration (200 $\mu g/mL$), underscoring their better biocompatibility. Upon light irradiation, both PS@BSA NPs caused substantial cell death, validating their great PDT efficacy. Live/dead staining assays further corroborated effective PDT result (**Figure 5E**), that are, when B16-F10 cancer cells uptake PS-1@BSA NPs and PS-2@BSA NPs, after a period of white light irradiation, a large area of cells showed obvious red fluorescence. It was directly proved that the prepared PS-1@BSA NPs and PS-2@BSA NPs had good PDT efficacy, which is expected to show great application potential for treating cancer.

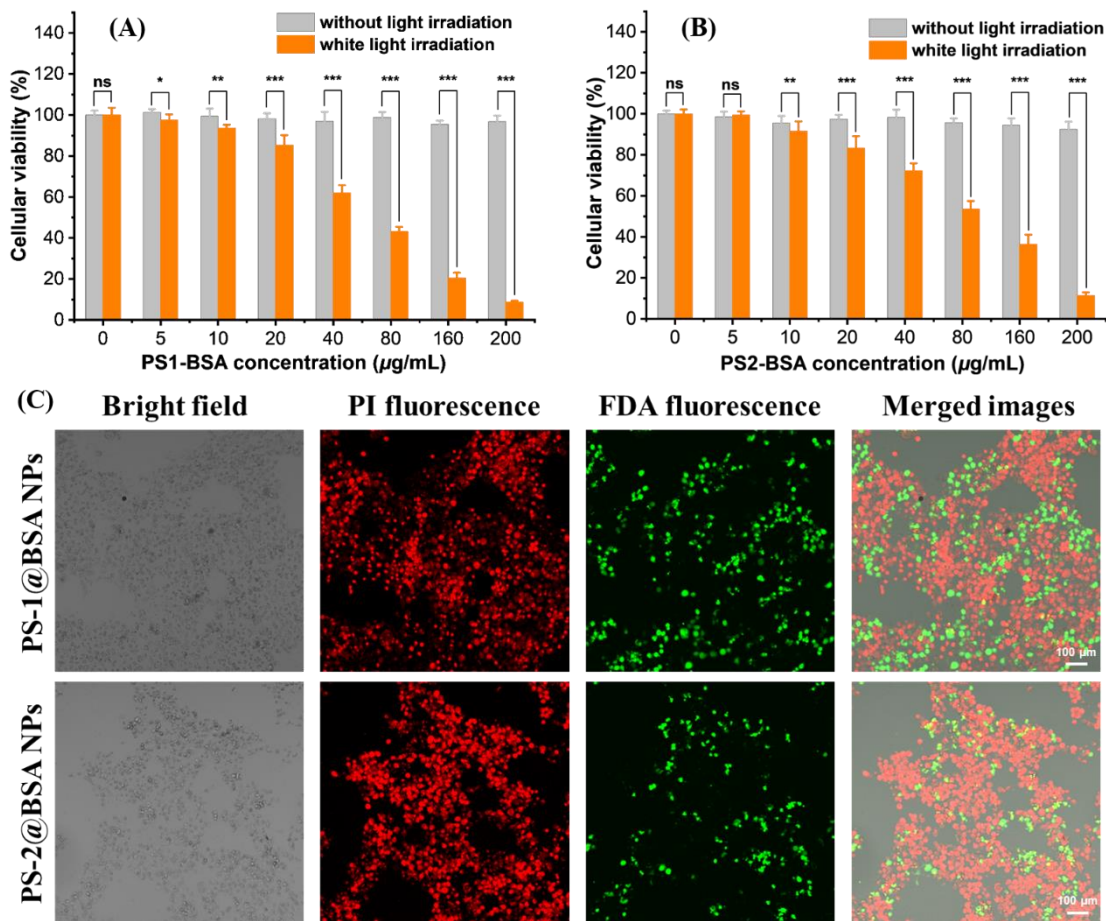


Figure 5 (A) PS-1@BSA NPs, (B) PS-2@BSA NPs against B16-F10 cancer cells at varying concentrations, (C) Live/dead cell costaining assays using FDA and Propidium iodide (PI) as fluorescence probes for PS-1@BSA NPs and PS-2@BSA NPs, scale bar: 100 μm , [PI] = 2 μM , [FDA] = 5 μM , [PS-1@BSA NPs] = 200 $\mu\text{g/mL}$, [PS-2@BSA NPs] = 200 $\mu\text{g/mL}$, white light: 30 mW cm^{-2} .

Conclusion

In summary, this work reported an effective click reaction to fabricate BSA encapsulates the AIE-active PS's NPs. Two alkynyl-contained AIE-active PSs with bright fluorescence and strong generating capability of type I/II ROS at aggregation were designed and synthesized, and their chemical structures were full confirmed by using $^1\text{H}/^{13}\text{C}$ NMR spectra and HRMS spectra. When mixing BSA and PS-1/PS-2 solution and receiving UV light irradiation, two stable PS-1@BSA NPs and PS-2@BSA NPs with

enhanced aqueous dispersibility and small size of near 100 nm were obtained, which could effectively produce type I ROS of O_2^- and $\cdot OH$, which showed good PDT efficacy to the B16-F10 cancer cells. This work proposed a universal and eco-friendly method for constructing hydrophilic AIE-active PS's NPs, which is expected to show huge promising potential for future biomedical applications.

Conflict of interest statement

There are no conflicts to declare.

Acknowledgements

This work is supported by Special fund for laboratory animals of Gansu Natural Science Foundation (24JRRA379), Foundation of Gansu Province (23JRRA1518), Provincial Talent Project of Gansu Province (GZTZ2024-4), Project of Gansu Provincial Department of Education (2023QB-056), Talent Innovation and Entrepreneurship Project of Lanzhou City (2022-RC-49), Talent Innovation and Entrepreneurship Project of Chengguan District (2022-rc-7), Scientific Research Fund Project of the Hospital(GMCCH2024-2-4).

References

- [1] Pham, T. C.; Nguyen, V.; Choi, Y.; Lee, S.; Yoon, J. Recent Strategies to Develop Innovative Photosensitizers for Enhanced Photodynamic

- Therapy. *Chem. Rev.* **2021**, *121*, 13454-13619.
- [2] Zhang, W.; Ahmed, A.; Cong, H.; Wang, S.; Shen, Y.; Yu, B. Application of multifunctional BODIPY in photodynamic therapy. *Dyes Pigments*. **2021**, *185*, 108937.
- [3] Algorri, J. F.; Ochoa, M.; Roldán-Varona, P.; Rodríguez-Cobo, L.; López-Higuera, J. M. In *Cancers*, 2021; Vol. 13.
- [4] Tao, T.; Hu, X.; Sun, D.; Ou, C.; Guo, Y.; Xu, H. The halogen effect of bis-truxene substituted BODIPY photosensitizers for potential photodynamic therapy. *Dyes Pigments*. **2024**, *224*, 111996.
- [5] Yu, Y.; Jia, H.; Liu, Y.; Zhang, L.; Feng, G.; Tang, B. Z. Recent Progress in Type I Aggregation-Induced Emission Photosensitizers for Photodynamic Therapy. *Molecules*, **2023**, *28*, 332.
- [6] Ni, J.; Wang, Y.; Zhang, H.; Sun, J. Z.; Tang, B. Z. Aggregation-Induced Generation of Reactive Oxygen Species: Mechanism and Photosensitizer Construction. *Molecules*, **2021**, *26*, 268.
- [7] Wang, X.; Yang, L.; Li, Y. H.; Wang, X. H.; Qi, Z. J. A Long-Retention Cell Membrane-Targeting AIEgen for Boosting Tumor Theranostics. *Chem-AsianJ.* **2024**, *19*, e202400305.
- [8] Wang, X.; Tang, Y. Q.; Liang, J. K.; Zhao, Y. F.; Yang, L.; Qi, Z. J. A lipid droplet-specific near-infrared automatic oxygen-supplied AIEgen for photodynamic therapy and metastasis inhibition of hypoxic tumors. *Chem. Eng. J.* **2023**, *453*, 139838.

- [9] Gao, J.; Tian, Y.; Li, Y.; Hu, F.; Wu, W. Design strategies for aggregation-induced emission photosensitizers with enhanced safety in photodynamic therapy. *Coord. Chem. Rev.* **2024**, *507*, 215756.
- [10] Wan, Q.; Li, Y.; Ding, K.; Xie, Y.; Fan, J.; Tong, J.; Zeng, Z.; Li, Y.; Zhao, C.; Wang, Z. et al. Aggregation Effect on Multiperformance Improvement in Aryl-Armed Phenazine-Based Emitters. *J. Am. Chem. Soc.* **2023**, *145*, 1607-1616.
- [11] Li, Y.; He, D.; Wan, Q.; Tang, B. Z.; Wang, Z. An innovative stepwise activated coupling reaction for fabricating functional fluorescence probes with potential photosensitive applications. *Sensor Actuator B-Chem.* **2024**, *412*, 135725.
- [12] Wang, X.; Li, Y. H.; Hasrat, K.; Yang, L.; Qi, Z. J. Sequence-Responsive Multifunctional Supramolecular Nanomicelles Act on the Regression of TNBC and Its Lung Metastasis via Synergic Pyroptosis-Mediated Immune Activation. *Small*, **2023**, *19*, 2305101.
- [13] Wang, X.; Li, Y. H.; Qi, Z. J. Light-Enhanced Tandem-Responsive Nano Delivery Platform for Amplified Anti-tumor Efficiency. *Chem-AsianJ.* **2024**, *19*, e202400311.
- [14] Zheng, Y.; Li, Y.; Bai, X.; Teng, M.; Tang, Y.; Zhao, S.; Ma, Z.; Liang, H.; Xie, Y.; Wan, Q. Atomic Engineering and Aggregation Effect to Regulate Synergistically Type I Reactive Oxygen Species of AIE-Active Deep Red/Near Infrared Red Photosensitizer. *Small* **2025**, *21*, 2410816.

- [15] Min, X.; Yi, F.; Han, X.; Li, M.; Gao, Q.; Liang, X.; Chen, Z.; Sun, Y.; Liu, Y. Targeted photodynamic therapy using a water-soluble aggregation-Induced emission photosensitizer activated by an acidic tumor microenvironment. *Chem. Eng. J.* **2022**, *432*, 134327.
- [16] Li, X.; Xiong, Y. Application of “Click” Chemistry in Biomedical Hydrogels. *ACS Omega* **2022**, *7*, 36918-36928.
- [17] Kaur, J.; Saxena, M.; Rishi, N. An Overview of Recent Advances in Biomedical Applications of Click Chemistry. *Bioconjug. Chem.* **2021**, *32*, 1455-1471.
- [18] Albada, B.; Keijzer, J. F.; Zuilhof, H.; van Delft, F. Oxidation-Induced “One-Pot” Click Chemistry. *Chem. Rev.* **2021**, *121*, 7032-7058.
- [19] McDaniel, R. M.; Carey, M. S.; Wilson, O. R.; Barsoum, M. W.; Magenau, A. J. D. Well-Dispersed Nanocomposites Using Covalently Modified, Multilayer, 2D Titanium Carbide (MXene) and In-Situ “Click” Polymerization. *Chem. Mat.* **2021**, *33*, 1648-1656.
- [20] Sradha S, A.; Sariga; George, L.; Varghese, A. Advancements in thiol-yne click chemistry: Recent trends and applications in polymer synthesis and functionalization. *Mater. Today Chem.* **2024**, *38*, 102112.
- [21] Lü, S.; Wang, Z.; Zhu, S. Thiol-Yne click chemistry of acetylene-enabled macrocyclization. *Nat. Commun.* **2022**, *13*, 5001.
- [22] Wang, B.; Li, C.; He, D.; Ding, K.; Tian, Q.; Feng, G.; Qin, A.; Tang, B. Z. Bioconjugation and Reaction-Induced Tumor Therapy via

- Alkynamide-Based Thiol-Yne Click Reaction. *Small* **2024**, *20*, 2307309.
- [23] Mitmoen, M.; Kedem, O. UV- and Visible-Light Photopatterning of Molecular Gradients Using the Thiol–yne Click Reaction. *ACS Appl. Mater. Interfaces* **2022**, *14*, 32696-32705.
- [24] Deng, D.; Yang, Y.; Liu, S.; Deng, X.; Chen, Z.; Pu, S. Benzothiadiazole-based dibenzobenzimidazole derivatives with aggregation-induced deep-red fluorescence and different mechanically responsive fluorescence features. *Dyes Pigments*. **2022**, *205*, 110580.
- [25] He, Y.; Xie, F.; Li, H.; Zhang, K.; Shen, Y.; Ding, F.; Wang, C.; Li, Y.; Tang, J. Red-shift emission and rapid up-conversion of B,N-containing electroluminescent materials via tuning intramolecular charge transfer. *Mater. Chem. Front.* **2023**, *7*, 2454-2463.
- [26] Long, J.; Shan, J.; Zhao, Y.; Ji, Y.; Tan, H.; Wang, H. Dramatically Enhanced and Red-shifted Photoluminescence Achieved by Introducing an Electron-withdrawing Group into a Non-traditional Luminescent Small Organic Compound. *Chem-Asian J.* **2021**, *16*, 2426-2430.
- [27] Wu, H.; Du, L.; Luo, J.; Wang, Z.; Phillips, D. L.; Qin, A.; Tang, B. Z. Structural modification on tetraphenylpyrazine: from polarity enhanced emission to polarity quenching emission and its intramolecular charge transfer mechanism. *J. Mater. Chem. C* **2022**, *10*, 8174-8180.
- [28] Wang, J. F.; Cao, M. Y.; Han, L. L.; Shangguan, P.; Liu, Y. S.; Zhong, Y.; Chen, C. Y.; Wang, G. Y.; Chen, X. Y.; Lin, M.; Lu, M. Y.; Luo, Z. Q.;

He, M.; Sung, H. H. Y.; Niu, G. L.; Lam, J. W. Y.; Shi, B. Y.; Tang, B. Z. Blood–Brain Barrier-Penetrative Fluorescent Anticancer Agents Triggering Paraptosis and Ferroptosis for Glioblastoma Therapy, *J. Am. Chem. Soc.* **2024**, *146*, 42, 28783–28794.

[29] Cao, S. X.; Tian, X. Y.; Cao, M. Y.; Wang, J. G.; Niu, G. L.; Tang, B. Z. Solvatochromic Near-Infrared Aggregation-Induced Emission-Active Acrylonitriles by Acceptor Modulation for Low-Power Stimulated Emission Depletion Nanoscopy, *Chem. Mater.* **2023**, *35*, 6, 2472–2485.

[30] Wan, Q.; Dai, W.; Xie, Y.; Ke, Q.; Zhao, C.; Zhang, B.; Zeng, Z.; Wang, Z.; Tang, B. Z. AIE-active deep red/near-infrared electroluminescent emitters with fine regulation of excited state. *Chem. Eng. J.* **2023**, *451*, 138529.

[31] Li, D.; Zuo, R.; Wang, J.; Le, Z. The Designs and Applications of Tetraphenylethylene Macrocycles and Cages. *Chem-Eur J.* **2025**, *31*, e202403715.

[32] Ito, F. Fluorescence Detection of Dynamic Aggregation Processes Using AIEgens, 2022.

[33] Huang, J.; Zhou, Y.; Wang, W.; Zhu, J.; Li, X.; Fang, M.; Wu, Z.; Zhu, W.; Li, C. A fluorescent probe based on triphenylamine with AIE and ICT characteristics for hydrazine detection. *Spectrochimica Acta Part a: Molecular and Biomolecular Spectroscopy* **2023**, *286*, 122011.

[34] Tang, Y.; Xie, Y.; Bai, X.; Zhao, C.; Zheng, Y.; Liang, H.; Ma, Z.;

Wang, Z.; Wan, Q. Building Block for Designing Bright Type I AIE-Active Photosensitizers with Deep/Near-infrared Red Fluorescence. *Chemistry – an Asian Journal* **2025**, *20*, e202401276.

[35] Wan, Q.; Zhang, R.; Zhuang, Z.; Li, Y.; Huang, Y.; Wang, Z.; Zhang, W.; Hou, J.; Tang, B. Z. Molecular Engineering to Boost AIE-Active Free Radical Photogenerators and Enable High-Performance Photodynamic Therapy under Hypoxia. *Adv. Funct. Mater.* **2020**, *30*, 2002057.